CLUMPED ISOTOPE THERMOMETRY IN DEEPLY BURIED SEDIMENTARY CARBONATES: THE EFFECTS OF BOND REORDERING KINETICS AND RECRYSTALLIZATION

A Thesis

by

BROCK J. SHENTON

Submitted to the Office of Graduate and Professional Studies of
Texas A&M University
in partial fulfillment of the requirements for the degree of

MASTER OF SCIENCE

Chair of Committee,	Ethan L. Grossman
Committee Members,	Deborah J. Thomas
	Michael C. Pope
Head of Department,	John R. Giardino

August 2014

Major Subject: Geology

ABSTRACT

I utilize clumped isotope thermometry to explore the diagenetic and thermal histories of exhumed brachiopods, crinoids, cements, and host rock in the Palmarito Formation, Venezuela and the Bird Spring Formation, Nevada, USA. Carbonate components in the Palmarito Formation, which experienced ~4 km of burial, yield statistically indistinguishable clumped isotope temperatures ($T(\Delta_{47})$s) ranging from 86 to 122 °C. Carbonate clumped isotope temperatures in the more deeply buried Bird Spring Formation (>5 km) range from ~100 to 165 °C and differ by component type, with brachiopods and pore-filling cements yielding the highest $T(\Delta_{47})$s (mean = 153 and 141 °C, respectively) and crinoids and host rock yielding significantly cooler $T(\Delta_{47})$s (mean 103 and 114 °C). New high-resolution thermal histories are coupled with kinetic models to predict the extent of solid-state C–O bond reordering during burial and exhumation for both sites. Application of these models, termed 'THRMs' (Thermal History Reordering Models), suggests that brachiopods in the Palmarito Formation experienced partial bond reordering without complete equilibration of clumped isotopes at maximum burial temperatures. In contrast, $T(\Delta_{47})$s of brachiopods from the Bird Spring Formation completely equilibrated at maximum burial temperatures, and reflect blocking temperatures achieved during cooling. Relative to the brachiopod calcite, the 40-50 °C cooler clumped isotope temperatures measured in Bird Spring Formation crinoids and host rock can be explained by recrystallization and cementation during shallow burial and a greater inherent resistance to solid-state reordering.

DEDICATION

To my mother

ACKNOWLEDGEMENTS

I would like to thank my committee chair, Ethan Grossman for his academic and personal mentorship. I thank committee members, Debbie Thomas and Mike Pope and acknowledge Juan Carlos Laya, Tom Yancey, Brent Miller, and Andy Kronenberg for discussions which guided and improved my research. I express sincere appreciation to Greg Henkes for accommodating me on visits to Johns Hopkins University and for his consistent interest and encouragement. I thank Ben Passey for offering his technical expertise and for analytical training. I acknowledge the assistance of Tom Becker, Steve Becker, and Michael Lawson at ExxonMobil Upstream Research Company in acquiring sample thermal histories. Finally, I thank Luz Romero for assistance with trace elemental analyses and Bob Reynolds for acquiring fluid inclusion microthermometry data.

I am grateful for scholarships from the Berg-Hughes Center for Petroleum Systems Analysis at Texas A&M University and for a fellowship from ConocoPhillips. This research was supported by a grant from the United States National Science Foundation (EAR-1227076) and a James E. Hooks Memorial Grant through the American Association of Petroleum Geologists Foundation Grants-in-Aid program.

TABLE OF CONTENTS

Page

LIST OF FIGURES

LIST OF TABLES

TABLE Page

1. INTRODUCTION

Constraining the diagenetic and thermal histories of sedimentary basins is fundamental to a range of geologic applications including tectonics, petroleum system analysis, and genesis of metallic ore deposits. A common way to reconstruct temperature-time (T-t) histories of sedimentary rocks is to use models calibrated by paleothermometry. This combined approach includes constructing a prograde burial history from the thicknesses, lithologies, and ages of overlying stratigraphic formations, with assumptions about radiogenic heat generation and basal heat flow through time. Ideally, models are calibrated by organic- or mineral-based thermal indicators such as vitrinite reflectance (e.g., Sweeney and Burnham, 1990), the conodont alteration index (e.g., Epstein et al., 1977), molecular biomarkers (e.g., Peters et al., 2005), or fluid inclusion microthermometry (e.g., Goldstein and Reynolds, 1994). Sediment cooling histories can then be approximated with thermochronometric tools such as fission-track analysis (e.g., Gleadow et al., 1986) or (U-Th)/He dating (e.g., Farley, 2002).

While these thermal indicators provide valuable model constraints, each tool is limited by material availability or its usable temperature range. Thus, it is important to explore emergent techniques, such as carbonate clumped isotope thermometry (Eiler, 2007; Eiler, 2011), which can be diversely applied to virtually any carbonate in a range of thermal settings. For example, the technique has been applied in the diagenetic temperature range (ca. 150 °C and lower) to reconstruct mineralization temperatures and to reveal fluid chemistries associated with cements and fractures (e.g., Huntington et al.,

2011; Budd et al., 2013; Loyd et al., 2013), faults (Swanson et al., 2012; Bergman et al., 2013), and concretions (Loyd et al., 2012; Dale et al., 2014). At higher temperatures, clumped isotopes may be useful for reconstructing cooling rates (e.g., Passey and Henkes, 2012) and refining burial histories (e.g., Henkes et al., 2014).

A primary way that carbonate rocks can serve as archives of basin thermal histories relates to solid-state reordering of C-O bonds at elevated temperatures (Dennis and Schrag, 2010; Passey and Henkes, 2012; Henkes et al., 2014). This process is inferred to involve breakage of existing C–O bonds, diffusive migration of C or O (or both) to new lattice coordinates, and reforming of new C–O bonds. Solid-state reordering tends to drive concentrations of isotopic clumps (e.g., ^{13}C–^{18}O bonds) towards equilibrium with the elevated temperature regime (Passey and Henkes, 2012; Henkes et al., 2014). Such closed-system alteration differs from open-system diagenesis (e.g., occlusion of pore space or dissolution-reprecipitation reactions) in that it can occur without imparting noticeable changes to bulk isotopic compositions ($\delta^{13}C$ and $\delta^{18}O$), elemental concentrations, or mineral texture. Laboratory heating experiments of calcites demonstrate that C-O bond reordering follows first-order reaction progress after an initial period of non-first-order behavior (Passey and Henkes, 2012). Arrhenius regressions of the experimental data allow for determination of kinetic parameters (e.g., activation energy, E_a and frequency factor, K_o), which in turn permit calculation of the extent of ^{13}C–^{18}O bond reordering at a given temperature during a given time interval (Passey and Henkes, 2012). The evolution of $T(\Delta_{47})$ during experimental heating has been modeled using a first-order approximation model (FOAM; Passey and Henkes,

2012), or a transient / equilibrium defect model (TED; Henkes et al., 2014), which accounts for the early non-first order kinetics observed in experimental data. Both kinetic models predict essentially identical bond reordering rates at temperatures below ~200 °C (Henkes et al., 2014).

More formally, the modeling of C–O bond reordering during geological heating and cooling circuits (e.g., burial and exhumation or heating and cooling during contact metamorphism) requires knowledge of, or assumptions about, the reordering kinetics of the mineral phase in question. This involves a specific rate law for the reordering reaction (and the corresponding integrated rate equation), as well as Arrhenius parameters specific to the mineral phase. Such kinetic models include the 'FOAM' and 'TED' models mentioned previously. Thermal history reordering models also require knowledge or assumptions about the temperature history of the mineral phase in question. In practice, the temperature history is discretized into a series of temperature-time steps, and the reordering rate equation is used to calculate the extent of clumped isotope reordering during each step. The 'new' $T(\Delta_{47})$ at the end of each step is treated as the 'initial' $T(\Delta_{47})$ for the next step. These models, here termed 'THRMs' (Temperature History Reordering Models), are initialized with a primary carbonate mineralization temperature, and assume that the mineral lattice remains intact during the heating and cooling event (i.e., no dissolution / reprecipitation, authigenic ingrowth of carbonate, or other means of destroying original mineral lattice and precipitating new lattice). Initial comparisons of THRM predictions to measured $T(\Delta_{47})$s of exhumed Carboniferous brachiopods, for a range of burial scenarios, show that where thermal histories are

reasonably well-characterized, there is general data-model agreement (Henkes et al., 2014).

A related but relatively unexplored observation is that different calcites can have different C-O bond reordering kinetics. Such differences are evident in Arrhenius parameters of a brachiopod, optical calcite, and vein-filling spar, which have similar activation energies (188-208 kJ/mol), but frequency factors that differ by approximately two orders of magnitude (Passey and Henkes, 2012; Henkes et al., 2014). Differences in bond reordering kinetics may result from different defect compositions of different calcites (e.g., vacancies, interstitials), as defects are thought to be the primary agents enabling solid-state diffusion, and hence breakage and reforming of C–O bonds, which is necessary for ^{13}C–^{18}O bond reordering (Passey and Henkes, 2012). This is consistent with laboratory observations in which an order of magnitude increase in Mn content in calcite (causing an increase in point defect concentration) results in an approximately five-fold increase of O self-diffusion (Kronenberg et al., 1984). While a better understanding of the mechanism(s) of C-O bond reordering will require further laboratory investigation, there is potential for components with significantly different mineralogy; major, minor or trace element geochemistry; or other properties to have significantly different C-O bond reordering kinetics. Such variability could result in different responses when subjected to the same thermal history. Fortunately, this potentiality can be tested geologically with diverse carbonate components (e.g., brachiopods, crinoids, cements, etc.) that have experienced substantial burial heating.

In this study I explore clumped isotope compositions of brachiopods, crinoids, pore-filling cements, and host rock in the Palmarito Formation, Venezuela and the Bird Spring Formation at Arrow Canyon, Nevada, USA. Both the Palmarito and Bird Spring formations experienced deep sedimentary burial (~4 and 5 km, respectively), such that burial heating is expected to alter Δ_{47} values via solid-state reordering (i.e., > ~100-120 °C; Henkes et al., 2014). Samples from both localities were collected from constrained stratigraphic intervals, ensuring that all components experienced identical burial temperature histories. I then present new thermal histories for both sites calibrated by independent thermal history tools. This allows for direct comparison of measured $T(\Delta_{47})$s of the different carbonate components to THRM predictions based on first-order kinetics and previously determined Arrhenius parameters. Guided by the data-model comparisons, I refine the compiled thermal histories and present hypotheses of component diagenetic histories and C-O bond reordering kinetics.

2. GEOLOGIC CONTEXT

2.1 Palmarito Formation, Venezuela

The Permian Palmarito Formation formed in the Mucuchachi Basin of northern Gondwana in the southern portion of the Venezuelan Andes (Fig. 1; Laya and Tucker, 2012). Sediments were likely deposited on a laterally extensive, northward-dipping homoclinal carbonate ramp (Laya and Tucker, 2012). Strata are cyclic (Laya et al., 2013b) and formed in various depositional settings ranging from deep subtidal to supratidal sequences. The Palmarito Formation is also rich in photozoan and heterozoan assemblages and deeper ramp facies contain occasional inter-bedded dolomite (Laya and Tucker, 2012). After burial in the Mucuchachi foreland basin, Neogene tectonism exhumed the Venezuelan Andes in distinct continental blocks (Colletta et al., 1997; Mann et al., 2006; Bermudez, 2010), which exposed the Palmarito Formation.

In building a burial temperature history for the Palmarito Formation, I assume that prograde burial history follows the path of Callejon et al. (2003), who synthesized a T-t history for the base of the overlying La Quinta Formation. Their model is modified here to include additional burial depth, including progressive compaction of the Palmarito Formation at the Quebrada de Portachuelo site (Fig. 1). Uncertainties for the prograde thermal history are based on low and high estimates of geothermal gradients (see 'Thermal History Workflows' in Appendix A for details). The cooling history and associated uncertainties are calibrated by apatite fission-track ages in the La Quinta Formation from the same tectonic exhumation block (Bermudez et al., 2010).

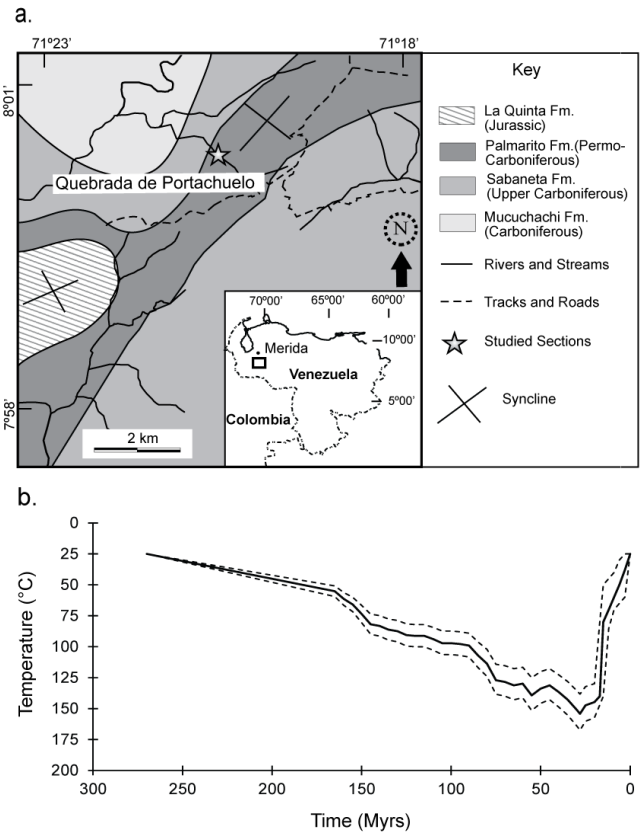

Fig. 1 Regional map and thermal history of Quebrada de Portachuelo area, Venezuela. (a) Geologic map showing the location of the collection site (denoted by a star) in northwest Venezuela, south of Merida modified from Laya et al. (2013b). (b) A temperature-time (T-t) history of the Permian Palmarito Formation at the Quebrada de Portachuelo (solid line). The prograde burial path is modified from Callejon et al. (2003) to account for additional burial depth of the Permian Palmarito Formation (which was not included in their work). The cooling history is compiled from Bermudez et al. (2013). Dashed lines are plotted to reflect thermal history uncertainties. Details of the T-t history compilation are outlined in Appendix A.

2.2 Bird Spring Formation, Nevada, USA

The Arrow Canyon Range is located in the eastern Great Basin Province in southeastern Nevada, USA (Fig. 2; Dickinson, 2006). Carboniferous sediments formed on a tropical carbonate platform in the Ely-Bird Spring Basin (EBSB; Stevens and Stone, 2007) with relatively continuous deposition, which contributed to its selection as the Global Stratotype Section and Point (GSSP) for the mid-Carboniferous boundary (Brenckle et al., 1997; Lane et al., 1999). Sediment packages are cyclothemic (Bishop et al., 2009; Bishop et al., 2010; Martin et al., 2012) and contain various shallow marine fauna including brachiopods, crinoids, corals and bryozoa (Langenheim, 1962; Brenckle et al., 1997; Lane et al., 1999; Richards et al., 2002; Bishop et al., 2009; Bishop et al., 2010). Meteoric cements fill primary and secondary porosity in laterally-extensive karstic and meteoric cementation horizons (Bishop et al., 2010). While the EBSB formed concurrently with other basins associated with the formation of the Ancestral Rocky Mountains (Kluth and Coney, 1981; Kluth, 1986; Dickinson and Lawton, 2003), it is likely not genetically-related, but rather formed as one of multiple foreland / forearc basins in Antler overlap sequences related to orogenesis in western Laurentia (Trexler et al., 2004; Cashman et al., 2011a; Cashman et al., 2011b; Sturmer, 2012). During the late Cretaceous, the Phanerozoic strata in the Arrow Canyon region were incorporated into the Sevier fold-and-thrust belt, which exhumed the EBSB interval and exposed it through erosive removal of most of the Permian and Mesozoic sections in southeastern Nevada (Page and Dixon, 1997).

The thermal history model for the Bird Spring Formation at Arrow Canyon, Nevada (Fig. 2) incorporates regional sediment thicknesses and was calibrated by peak temperature estimates from fluid inclusion microthermometry (T. Becker, personal communication, 2014). The cooling history at Arrow Canyon is built on the observation that the youngest concordantly folded strata in the region are of early-Late Cretaceous age (Fleck and Carr, 1990), which implies timing of deformation and uplift.

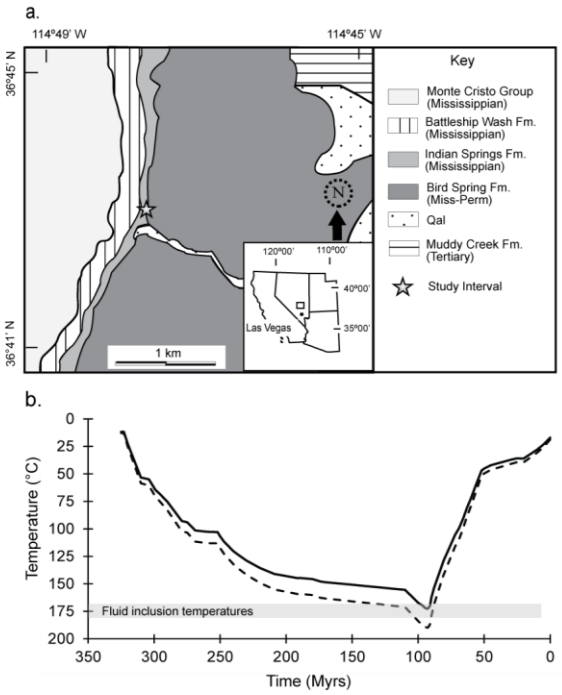

Fig. 2 Regional map and thermal history at Arrow Canyon, Nevada, USA**.** (a) Simplified geologic map showing the location of the collection site (denoted by a star) in the Bird Spring Formation after Cassity and Langenheim (1966). (b) A temperature-time history of the Mississippian-Pennsylvanian boundary at this locality (T. Becker, personal comm., 2014) is also shown (solid black line) with a 10% warmer thermal history plotted (dashed line) to demonstrate uncertainty. Note that no cool thermal history scenario is plotted because fluid inclusion microthermometry precludes any cooler peak temperature than 170 °C. Details about thermal history compilations are described in Appendix A.

3. MATERIALS

3.1 Sample Collection

Carbonates from both localities (Fig. 3) were collected from the same stratigraphic intervals to ensure all components experienced identical burial histories. Samples were collected within ~165 m of the base of the Palmarito Formation at the Quebrada de Portachuelo, Venezuela (Laya and Tucker 2012; Laya et al., 2013a; Laya et al., 2013b) and within ~50 m of the GSSP in the Bird Spring Formation. A single exception is brachiopod sample A322, collected ~500 m up-section in the Bird Spring Formation.

3.2 Carbonate Components

3.2.1 Brachiopods

Fossil brachiopods are abundant in shallow marine facies throughout the Paleozoic and are composed of relatively large low-Mg calcite (LMC) shells which are resistant to diagenetic recrystallization (e.g., Popp et al., 1986; Grossman, 1994; Mii et al., 1999; Veizer et al., 1999; Fig. 3a-b). Texturally well-preserved brachiopods show promise as clumped isotope archives of sedimentary burial history because, assuming no cryptic recrystallization, any elevated T(Δ_{47}) (i.e., above the temperatures expected for precipitating seawater) is expected to be the result of C-O bond reordering. In addition, bond reordering kinetics of a well-preserved Late Paleozoic (Permian) brachiopod have already been determined in the laboratory (Henkes et al., 2014).

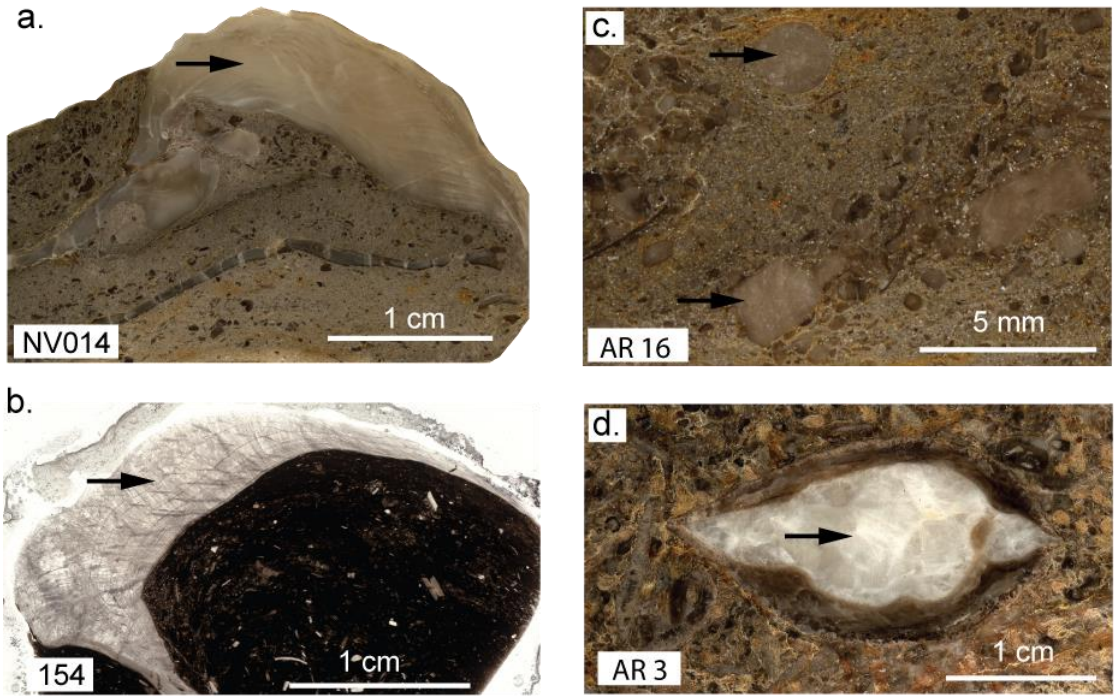

Fig. 3 Photomicrographs and thin section scans of carbonate components. Images include (a) a brachiopod sample from the Bird Spring Formation, Nevada, (b) a brachiopod sample from the Palmarito Formation, Venezuela, (c) crinoid ossicles (arrows) from the Bird Spring Formation, Nevada and (d) a sparry pore-filling cement within an articulated brachiopod shell from the Bird Spring Formation**.**

3.2.2 Crinoids

Crinoids originally consist of a polycrystalline high-Mg calcite (HMC) skeleton that behaves optically as a single crystal (Smith, 1990; Fig. 3c). Due to relatively high solubility of HMC in meteoric fluids, crinoids are susceptible to post-mortem stabilization to diagenetic low-Mg calcite (dLMC). The inversion occurs via open-system dissolution / reprecipitation reactions (Bischoff et al., 1993), and in crinoids is commonly accompanied by textural changes (Dickson, 2001). Such recrystallization is expected to alter the primary T(Δ_{47})s in the event that it occurs at a temperature that differs from the primary mineralization temperature of the crinoid. In addition, pore space of crinoids commonly exceeds 50% (Savarese et al., 1997) and may experience secondary infill, which would also change the bulk T(Δ_{47}) of the sample. In a simplified scenario, crinoidal T(Δ_{47})s likely increase early during burial due to calcite stabilization and porosity occlusion (herein referred to as 'stabilization temperature'), and may subsequently evolve during further heating due to solid-state C-O bond reordering.

3.2.3 Cements in Articulated Brachiopod Shells

Macroscopic, sparry cements enclosed by brachiopod shells at Arrow Canyon (Fig. 3d) are observed in laterally-extensive karstic or meteoric cementation horizons (Bishop et al., 2010) and likely formed early at near Earth-surface temperatures. Cements targeted for sub-sampling are encased by articulated LMC brachiopod shells which may act as low permeability barriers from external fluids, probably increasing the likelihood of preservation of primary bulk isotopic composition. Such cements were not observed in the Palmarito Formation.

3.2.4 Host Rock

Host rock is polygenetic by nature and the samples presented here range in texture from bioclastic wackestone to grainstone (Dunham, 1962). Host rock was likely originally composed, at least in part, of aragonite or HMC and is expected to experience chemical and structural diagenesis during burial. Clumped isotope temperatures of host rock are expected to be similar to the temperature of porosity-fill, cementation, inversion to dLMC, and compaction and are susceptible to subsequent alteration from C-O bond reordering during deep burial.

3.3 Sample Characterization

Thin sections of carbonate components were characterized using optical and cathodoluminescence microscopy with a TECHNOSYN Model 8200 MKII luminoscope at Texas A&M University. The luminoscope was operated between 200 and 300 mA and 10-15 kV and images were taken with a Coolsnap-Pro_{cf} digital camera with exposure times ranging from 20 to 30 seconds. Cathodoluminescence is a commonly applied technique used to identify recrystallization, as luminescence is a function of elevated concentrations of diagenetic trace metals, primarily Mn^{2+} (Pierson, 1981; Machel, 1985). Based on the petrographic observations, carbonate powders were milled with 0.5 mm or 1 mm dental burs and homogenized prior to aliquoting for elemental and isotopic analyses. Caution was used to characterize and sub-sample brachiopod shells, which were qualitatively

designated as non-luminescent (NL), slightly-luminescent (SL), or cathodoluminescent (CL; Fig. 4). To fully characterize the potential influence of open-system alteration (i.e. recrystallization), elemental and isotopic analyses were performed on samples of differing luminescence character. Because host rock, crinoids, and cements are susceptible to post-depositional alteration, the presence or absence of luminescence was not a precondition for sub-sampling. Due to the small size of crinoids and the relatively large sample size required for clumped isotope analysis, some sample powders were drilled and homogenized from multiple adjacent ossicles (e.g., samples AR7, AR8, and AR16). All crinoids show loss of primary stereom microstructure and some have abundant micro-fractures (e.g., AR8 and AR12; Fig. A-1). Crinoids at the Quebrada de Portachuelo site were exceptionally scarce, resulting in analyses of only two samples without complementary thin sections and trace element analyses. Host rock samples were characterized according to depositional texture (Dunham, 1962; Fig. A-2, 3).

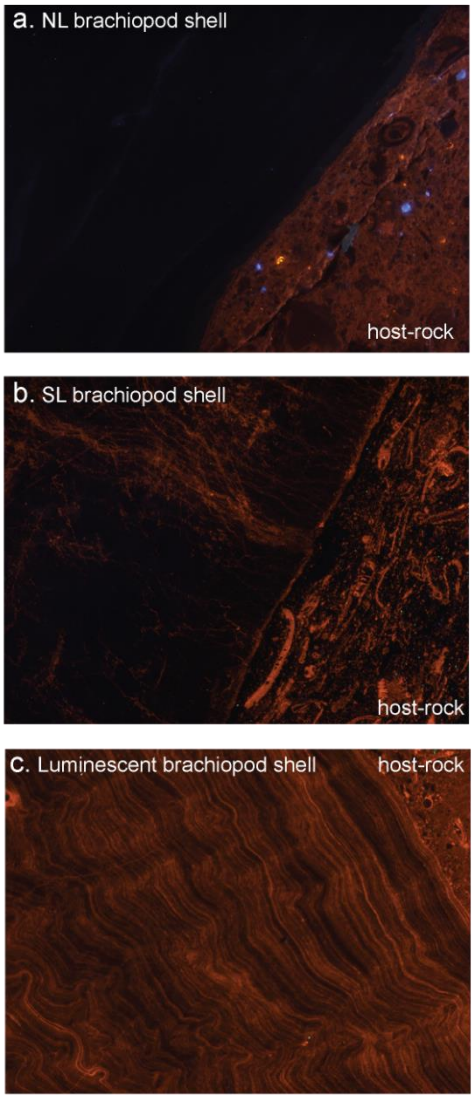

Fig. 4 Cathodoluminescence microscopy of brachiopod shells. Cathodoluminescence images of brachiopod shells include qualitative descriptions including (a) non-luminescent (NL; sample NV014), (b) slightly-luminescent (SL; 152), and (c) cathodoluminescent (CL; 144). Scale for each image is ~3.25 mm

4. ANALYTICAL METHODS

4.1 Elemental Analysis

For elemental analyses (Ca, Sr, Mg, Mn, and Fe), aliquots of ~100 µg of sample powder were reacted in 2 ml of HNO_3 for > 1 hour prior to analysis on a Thermo Scientific Element XR high-resolution inductively coupled plasma mass spectrometer (HR-ICP-MS) at Texas A&M University. To correct for instrument drift, ~0.2 ml of indium was also added to each solution. Analytical sessions included measurements of internal standards with known elemental concentrations as well as MACS-3, a USGS prepared marine carbonate standard. In rare instances the homogenized sample powder was of insufficient mass, requiring additional milling of ~100 µg of powder from the identical position on the adjacent sample billet.

4.2 Stable Isotope Measurements

Isotopic analyses ($\delta^{13}C$, $\delta^{18}O$, and Δ_{47}) were performed at Johns Hopkins University (JHU) on a Thermo Finnigan MAT 253 isotope ratio mass spectrometer (IRMS) connected to a custom-built, automated acid digestion and sample purification line. Clumped isotope measurements involved an 'online' reaction of ~7-8 mg of calcite in a common acid bath with concentrated H_3PO_4 at 90 °C during two analytical sessions in Spring and Fall, 2013. Analytical procedures and data normalization approaches are

detailed in Henkes et al. (2013). Most measurements were made on three different aliquots of the same carbonate powder, which allowed for sufficient cumulative instrument counting time to approach the asymptotic portion of the carbonate clumped isotope shot-noise curve (e.g., Thiagarajan et al., 2011). Thus, total sample sizes of ~20-25 mg were required; however, as this was not always possible (e.g., for certain small crinoids), some samples were only analyzed once or twice.

Sub-daily measurements of CO_2 gases with known $\delta^{13}C$ and $\delta^{18}O$ values equilibrated at 30 °C and 1000 °C were also made to observe instrument linearity and to generate an empirical transfer function which allows for presenting data in an absolute reference frame herein referred to as the carbon dioxide equilibrium scale or 'CDES' (Dennis et al., 2011). This correction scheme empirically accounts for changes in ion source conditions as well as other mass spectrometer-specific artifacts (Dennis et al., 2011). During the spring 2013 session the heated gas slope, which defines the empirical transfer function, was observed to migrate through time. Thus, a 'moving' data correction scheme was applied to correct for the temporally-evolving non-linearity using a MATLAB script described in Passey et al. (2010). Isotopic compositions of internal

standards HAF-Carrara and 102-GC-AZ01 were also frequently measured during analytical sessions. Combined over both sessions, HAF-Carrara (n=15) yielded Δ_{47}, $\delta^{13}C$, and $\delta^{18}O$ values of 0.403 ± 0.013‰, 2.30 ± 0.04‰, and -1.82 ± 0.05‰, respectively (± values are 1σ) and 102-GC-AZ01 (n=15) yielded Δ_{47}, $\delta^{13}C$, and $\delta^{18}O$ values of 0.709 ± 0.013‰, 0.49 ± 0.06‰, and -14.47 ± 0.07‰. Clumped isotope temperatures are calculated using the theoretical predictions for temperature-dependent isotopic clumping in calcite by Schauble et al. (2006), adjusted for the equivalent CO_2 generated by acid digestion of calcite (Guo et al., 2009). Bulk isotope ($\delta^{13}C_{calcite}$ and $\delta^{18}O_{calcite}$) values are reported versus VPDB. $\delta^{18}O_{water}$ compositions are reported on the VSMOW scale and are calculated using $T(\Delta_{47})$ and associated $\delta^{18}O_{calcite}$ values applied to the calcite-water oxygen isotope thermometry equation of Friedman and O'Neil (1977).

5. RESULTS

Table 1 shows the results of the geochemical analyses of the carbonate components from the Palmarito Formation, Venezuela and the Bird Spring Formation at Arrow Canyon, Nevada, including isotopic ($\delta^{13}C_{calcite}$, $\delta^{18}O_{calcite}$, Δ_{47}) compositions, elemental (Mg, Sr, Mn, and Fe) concentrations, and calculated T(Δ_{47}), and $\delta^{18}O_{water}$ values. Bulk and clumped isotope data from four brachiopod and three host rock samples reported in Henkes et al. (2014) also are presented here, along with new elemental data.

5.1 Palmarito Formation, Venezuela

At Quebrada de Portachuelo, Venezuela, carbonate Δ_{47} values of components range between 0.481 ± 0.010‰ and 0.537 ± 0.025‰, corresponding to temperatures ranging from 86 ± 13 to 122 ± 7 °C (Fig. 5). Brachiopod apparent T(Δ_{47})s (94 ± 5 to 122 ± 7 °C) and calculated $\delta^{18}O_{water}$ values (8 ± 1 to 12 ± 1‰) are obviously elevated from expected mineralization temperatures and isotopic compositions of tropical Permian seawater (Fig. 1). High apparent T(Δ_{47})s are observed in NL and SL brachiopod shells, despite the observation of low Mn (< 115 ppm) and Fe (<186 ppm) concentrations, suggesting that the shells were not affected by bulk dissolution / reprecipitation. The CL brachiopod has a similar T(Δ_{47}) and has luminescence patterns that appear to follow growth bands (Fig. 4c) and may be primary. However, the shell has subtly elevated Mn and Fe concentrations with an obviously lower $\delta^{18}O_{calcite}$ value than the NL and SL

Sample ID	Carbonate phase	Relative position (m)*	n	$\delta^{13}C_{calcite}$ (‰, VPDB)	$\delta^{18}O_{calcite}$ (‰, VPDB)	Δ_{47} (CDES, ‰)†	Temp (°C) §	$\delta^{18}O_{water}$ (‰, VSMOW)#	Mg (ppm)	Sr (ppm)	Mn (ppm)	Fe (ppm)
Palmarito Formation, Venezuela												
141	Brachiopod (SL)**	37.0	3	4.13 ± 0.03	-3.70 ± 0.03	0.481 ± 0.010	122 ± 7	12 ± 1	845	761	115	186
144	Brachiopod (CL)	78.5	3	1.97 ± 1.04	-6.25 ± 0.09	0.507 ± 0.016	104 ± 10	8 ± 1	2430	911	188	356
152	Brachiopod (NL)	148.0	3	4.38 ± 0.02	-3.53 ± 0.04	0.503 ± 0.010	106 ± 6	10 ± 1	973	712	1	40
154	Brachiopod (SL)	167.2	3	4.34 ± 0.01	-3.94 ± 0.07	0.523 ± 0.008	94 ± 5	9 ± 1	964	842	22	137
141-Cr	Crinoid	60.0	1	2.89 ± 0.12	-7.92 ± 0.14	0.519 ± 0.025	96 ± 14	5 ± 1	-	-	-	-
141-Cr2	Crinoid	60.0	1	2.45 ± 0.12	-7.86 ± 0.14	0.537 ± 0.025	86 ± 13	4 ± 1	-	-	-	-
141-m	Wackestone (CL)††	60.0	2	1.34 ± 0.08	-7.63 ± 0.10	0.535 ± 0.018	87 ± 11	4 ± 1	2398	313	648	7066
144-m	Wackestone (CL)	78.5	2	2.73 ± 0.08	-7.95 ± 0.10	0.537 ± 0.018	86 ± 11	4 ± 1	4703	797	988	12800
Bird Spring Formation, NV, USA												
NV007	Brachiopod (NL)	-0.8	3	2.66 ± 0.05	-1.06 ± 0.04	0.439 ± 0.012	157 ±12	17 ± 1	2596	1146	23	14
NV008	Brachiopod (NL/SL)	-0.8	3	2.84 ± 0.03	-1.04 ± 0.03	0.430 ± 0.013	166 ± 13	18 ± 1	2032	809	5	58
NV013	Brachiopod (NL)	25.0	3	3.52 ± 0.01	-1.71 ± 1.02	0.453 ± 0.002	144 ± 2	16 ± 1	549	973	2	25
NV014	Brachiopod (NL)	33.5	3	1.55 ± 0.04	-0.78 ± 0.07	0.448 ± 0.005	148 ± 4	17 ± 1	2263	703	2	16
NV021	Brachiopod (NL/SL)	46.7	3	2.32 ± 0.04	-0.40 ± 0.04	0.461 ± 0.013	137 ± 11	17 ± 1	921	697	2	109
A322	Brachiopod (NL)	~500	2	3.42 ± 0.08	-1.65 ± 0.10	0.432 ± 0.018	164 ± 19	17 ± 1	461	1036	1	10
AR7	Crinoid (CL)	1.2-19	2	0.95 ± 0.08	-3.49 ± 0.10	0.518 ± 0.018	97 ± 11	10 ± 1	8300	487	958	2130
AR8	Crinoid (SL)	18.0	2	3.46 ± 0.08	-4.03 ± 0.10	0.515 ± 0.018	99 ± 11	9 ± 1	2440	252	9	24
AR12	Crinoid (SL)	7.5	3	3.28 ± 0.08	-3.55 ± 0.08	0.498 ± 0.015	110 ± 11	11 ± 1	8586	383	15	43
AR16	Crinoid (SL)	33.5	2	2.07 ± 0.08	-3.55 ± 0.10	0.500 ± 0.018	108 ± 13	10 ± 1	7969	605	14	54
AR3	Cement (CL)	-7.5	3	0.74 ± 0.02	-4.64 ± 0.19	0.462 ± 0.008	136 ± 7	12 ± 1	973	124	189	496
AR10	Cement (CL)	18.0	2	-0.69 ± 0.08	-5.17 ± 0.10	0.466 ± 0.018	133 ± 15	11 ± 1	113	16	19	18
AR13	Cement (CL)	-7.5	3	-0.66 ± 0.01	-4.53 ± 0.03	0.441 ± 0.009	155 ± 12	14 ± 1	733	158	126	90
AC1	Cement (CL)	20.3	2	0.74 ± 0.08	-4.37 ± 0.10	0.457 ± 0.018	141 ± 16	13 ± 1	1153	146	116	22
NV008-m	Wackestone (CL)	-0.8	3	-0.25 ± 0.11	-4.52 ± 0.00	0.504 ± 0.003	106 ± 2	9 ± 1	1891	171	52	2325
NV009-m	Packestone (CL)	4.2	2	1.17 ± 0.08	-3.65 ± 0.10	0.480 ± 0.018	123 ± 14	12 ± 1	2114	197	81	1111
NV014-m	Packestone (CL)	33.5	3	1.50 ± 0.03	-3.83 ± 0.02	0.509 ± 0.007	102 ± 5	10 ± 1	6202	434	24	464
NV021-m	Packestone (CL)	46.7	3	2.48 ± 0.03	-2.51 ± 0.12	0.474 ± 0.008	127 ± 6	13 ± 1	4360	470	51	321
AR2	Void-fill	-16.0	1	-0.56 ± 0.12	-15.33 ± 0.14	0.696 ± 0.025	21 ± 8	-14 ± 2	1829	115	2	13

Note: Where n ≥ 3, ± values of $\delta^{13}C$, $\delta^{18}O$ and Δ_{47} are reported as standard deviations of replicate analyses. Where n < 3, ± values are reported as 95 % confidence intervals for the standard deviation of the standards (δ13C = 0.06, δ18O = 0.017, and Δ47 = 0.013). Thus, for $\delta^{13}C$, ± values are 0.12 and 0.08 for n=1 and 2, respectively. For $\delta^{18}O$ ± values are 0.14 and 0.10 for n=1 and 2, respectively. For Δ_{47} ± values are 0.025 and 0.018 for n=1 and n=2.

*Relative position compared to the base of the Palmarito Formation for Venezuelan samples and compared to the Mississippian-Pennsylvanian boundary for samples from Nevada.

†Presented in the carbon dioxide equilibrium scale (Dennis et al., 2011) based on measurements of CO_2 gases equilibrated at 30 ° and 1000 °C. All values have been adjusted + 0.092 ‰ to correct for fractionation during acid digestion.

§Temperatures calculated using theoretical approximations of Schauble et al. (2006) corrected for acid digestion temperature of 90 °C (Guo et al., 2009).

#Isotopic compositions of waters were calculated using Friedman and O'Neil (1977).

**Qualitative descriptions of the cathodoluminescence character: non-luminescent (NL), slightly luminescent (SL), and luminescent (CL).

††Description of host-rock samples based on the carbonate classification scheme of Dunham (1962).

Table 1 Isotopic and elemental results from the Palmarito and Bird Spring formations.

shells, indicative of open-system diagenesis (Fig. 5). Palmarito crinoid and host rock samples yield mean T(Δ_{47})s of 91 and 87 °C, respectively. As expected, host rock samples have high concentrations of Mg, Mn and Fe with depleted Sr and $\delta^{18}O_{calcite}$, consistent with significant open-system alteration (Brand and Veizer, 1986).

5.2 Bird Spring Formation, Nevada

At Arrow Canyon, Nevada, Δ_{47} values of carbonate components range from 0.430 ± 0.013‰ to 0.696 ± 0.025‰, corresponding to a temperature range of 21 ± 8 °C to 166 ± 13 °C. With the exception of macro-scale calcite crystals filling presumably modern or recent dissolution vugs (Fig., A-6), all components collected near the GSSP yield clumped isotope temperatures in excess of ~95 °C, reflective of clumped isotopic signatures associated with deep sedimentary burial. Individual components (e.g., brachiopods, crinoids, etc.) cluster in distinct groups in a plot of T(Δ_{47}) versus $\delta^{18}O_{water}$ (Fig. 5). Arrow Canyon brachiopods yield the highest T(Δ_{47})s (mean = 153 °C), and the sparry cements which fill their shell interior have similar clumped isotope temperatures (mean = 141 °C). In contrast, crinoid and host rock T(Δ_{47})s (mean = 103 and 114 °C, respectively) are significantly cooler than brachiopod T(Δ_{47})s ($p = 0.0002$; Student's t-test) and interior cement T(Δ_{47})s ($p = 0.001$).

Similarly, elemental analyses show minor and trace element chemistries that differ between different carbonate components (Table 1). Arrow Canyon brachiopods have low concentrations of Mn and Fe (<23 ppm Mn and <109 ppm Fe) and relatively high concentrations of Sr, which are consistent with excellent bulk sample preservation. Crinoids have varying concentrations of Mg (2440-8586 ppm) and most samples have

low concentrations of Mn and Fe; however, crinoid sample AR7 is a notable exception containing ~1000 ppm Mn and >2100 ppm Fe. Host-rock samples also have relatively low concentrations of Mn, but on average yield the highest Fe concentrations. Pore-filling cements in articulated brachiopod shells have low concentrations of Mn and Fe and are depleted in Sr and $\delta^{18}O_{calcite}$, suggesting precipitation from a meteoric source

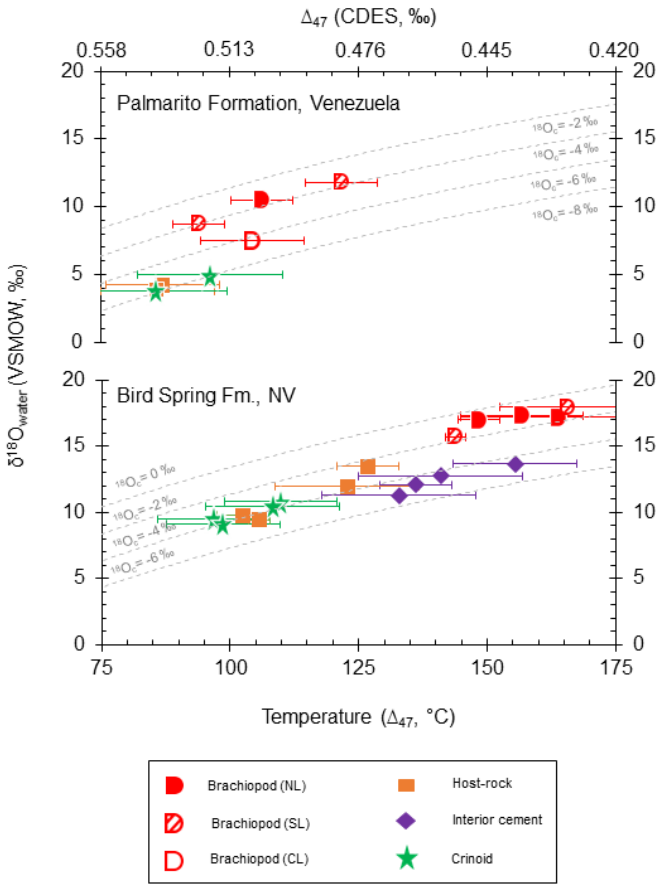

Fig. 5 $^{18}O_{water}$ vs clumped isotope temperature plot for carbonate components from the Palmarito Formation, Venezuela and the Bird Spring Formation, Nevada, USA. Grey dashed lines represent constant $^{18}O_{calcite}$ values (Friedman and O'Neil, 1977). Temperature uncertainties are based on the standard deviations of replicate analyses where $n \geq 3$ and 95 % confidence intervals for the standard deviation (0.013) of standards for samples where $n \leq 2$.

6. DISCUSSION

Given that the Palmarito and Bird Spring formations experienced substantial burial heating above the minimum temperatures necessary for solid-state alteration of Δ_{47} (i.e., ~100 to 120 °C; Henkes et al. 2014), it is not surprising that their carbonate components yield high apparent clumped isotope temperatures. Note that the NL and SL brachiopod shells (suggesting preservation from bulk dissolution / reprecipitation) from both localities track along 'closed-system pathways' in a plot of $\delta^{18}O_{water}$ versus temperature (Fig. 5; Henkes et al., 2014). This trend arises when Δ_{47} values are altered while simultaneously maintaining near primary $\delta^{18}O_{calcite}$ values, and is indicative of solid-state reordering of Δ_{47} or cryptic recrystallization by rock-buffered fluids.

Apparent clumped isotope temperatures of Palmarito brachiopods (94 ± 5 to 122 ± 7 °C) at the Quebrada de Portachueleo site are higher than T(Δ_{47})s of brachiopods from shallowly buried localities (e.g., ~20-40 °C; Came et al., 2007; Finnegan et al., 2011; Brand et al., 2012; Henkes et al., 2014). However, these Palmarito Formation brachiopod T(Δ_{47})s are lower than reported blocking temperatures of slowly cooled marbles (e.g., > ~150 °C; Ghosh et al., 2006), lower than calculated blocking temperatures (~150 °C) for extremely slowly-cooled calcites (≤ 10-7 °C/yr; Passey and Henkes, 2012), and lower than T(Δ_{47})s of extensively reordered brachiopods from Arrow Canyon, Nevada and the Uralian foredeep (e.g., ~ 140-165 °C; Henkes et al., 2014). Thus, Palmarito brachiopod shells may have experienced significant bond reordering, but did not reach thermal equilibrium at maximum burial temperatures. Bird Spring

Formation brachiopods (137 ± 11 to 166 ± 13 °C), which include four measurements from Henkes et al. (2014), are consistent with more substantial Δ_{47} alteration.

It is also not surprising that different carbonate components yield different clumped isotope temperatures (Fig. 5). Differences are expected to be related to brachiopods, crinoids and host rock having varying primary mineralogy and primary porosity, allowing for varied propensities for dissolution / reprecipitation style diagenesis as well as the potential for different C-O bond reordering kinetics. Thus, while brachiopods, crinoids, and host rock formed at approximately the same temperature and experienced identical burial temperature histories, the properties of the components result in different T(Δ_{47})-time responses. The apparent T(Δ_{47})s of these carbonates are an integration of 1) initial precipitation temperature, 2) temperature, timing and extent of recrystallization or secondary infill and 3) extent of solid-state C-O bond reordering, which depends on the thermal history and component-specific C-O bond reordering kinetics. Here I use THRMs to predict the extent of C-O bond reordering given the sample thermal histories.

6.1 Thermal History Reordering Models

Thermal history reordering models were used to evaluate the extent of C-O bond reordering in the Palmarito and Bird Spring formations. Models for both localities are initiated at 25 °C, consistent with plausible temperature estimates for precipitation in equatorial Paleozoic seas. Reordering models for the Palmarito and Bird Spring formations are initialized at 270 Ma and 325 Ma, respectively, according to independently constrained depositional ages (Laya et al., 2013; Page et al., 2005). I then

use equation 13 of Passey and Henkes (2012), which is based on first-order approximation kinetics with phase-specific E_a and K_o values to predict Δ_{47} values and associated T(Δ_{47})s at sequential time steps determined by the resolution of the compiled thermal histories. The final predicted T(Δ_{47}) (i.e., at the present day) can then be directly compared to the measured T(Δ_{47})s of exhumed carbonate components. Procedures and inputs for each of the following THRMs including kinetic model used, E_a, and K_o are presented in Table 2. For description of the derivation of the kinetic model and determination of sample Arrhenius parameters see Passey and Henkes (2012) and Henkes et al. (2014).

6.2 Data-Model Comparison

6.2.1 Palmarito Formation, Venezuela

The hypothesis of partial equilibration of clumped isotopes during burial is supported by a THRM based on an intermediate T-t history of the Palmarito Formation (Fig. 6b; termed THRM-Palmarito in Table 2). In the intermediate T-t scenario, a THRM predicts that samples experienced a finite amount of bond reordering and reached 117 °C (in terms of apparent T(Δ_{47})) during heating, which is within the range of measured T(Δ_{47})s of carbonate components (86-122 °C). In contrast, THRMs of the cool and warm scenarios of the Palmarito T-t history predict widely divergent T(Δ_{47})s. In the cool scenario, which reaches 138 °C peak temperature, the model predicts minimal bond reordering (Fig. 6a). In the warm scenario, which reaches 167 °C, the model predicts complete equilibration with a subsequent cooling-rate-dependent blocking temperature (Fig. 6c). Thus, uncertainties in the compiled thermal history of the Palmarito

Model name	Kinetic model	Material(s)	Activation Energy (kJ/mol) †	Frequency factor (s^{-1}) †
THRM-Palmarito	First-order approximation model*	Brachiopod calcite	188	4.45×10^{8}
THRM-Bird Spring	First-order approximation model	Brachiopod calcite	188	4.45×10^{8}
THRM-Stabilization	First-order approximation model	Brachiopod calcite	188	4.45×10^{8}
		Optical calcite	197	1.39×10^{9}
		Spar (labile)	208	5.6×10^{-9}
		Spar (refractory)	200	4.4×10^{7}

*Based on first-order approximation rate law and integrated rate equation of Passey and Henkes (2012)
†Experimentally determined in Passey and Henkes (2012) and Henkes et al. (2014)

Table 2 Thermal history reordering model parameters

Formation cause large differences in predicted clumped isotope temperatures, but the total range of predicted T(Δ_{47})s bracket the measured clumped isotope temperatures.

The widely divergent THRM predictions for the cool and warm T-t scenarios are related to a threshold behavior of C-O bond reordering which stems from rapid T(Δ_{47}) change in response to small changes in ambient temperature or dwelling time, particularly in the ~130-160 °C temperature range (Henkes et al., 2014). In this case, threshold behavior is advantageous because the data-model agreement in the intermediate T-t scenario validates that thermal history and casts doubt on more extreme cool and warm thermal scenarios. Similar treatments to refine thermal histories with peak temperatures in the ~130-160 °C range have obvious application because this temperature range coincides with the upper limits of the thermal window for oil generation and the lower limits for gas generation (Selley, 1998).

An inherent assumption in the THRM for the Palmarito Formation is that the carbonate components formed at 25 °C and did not recrystallize during burial. This

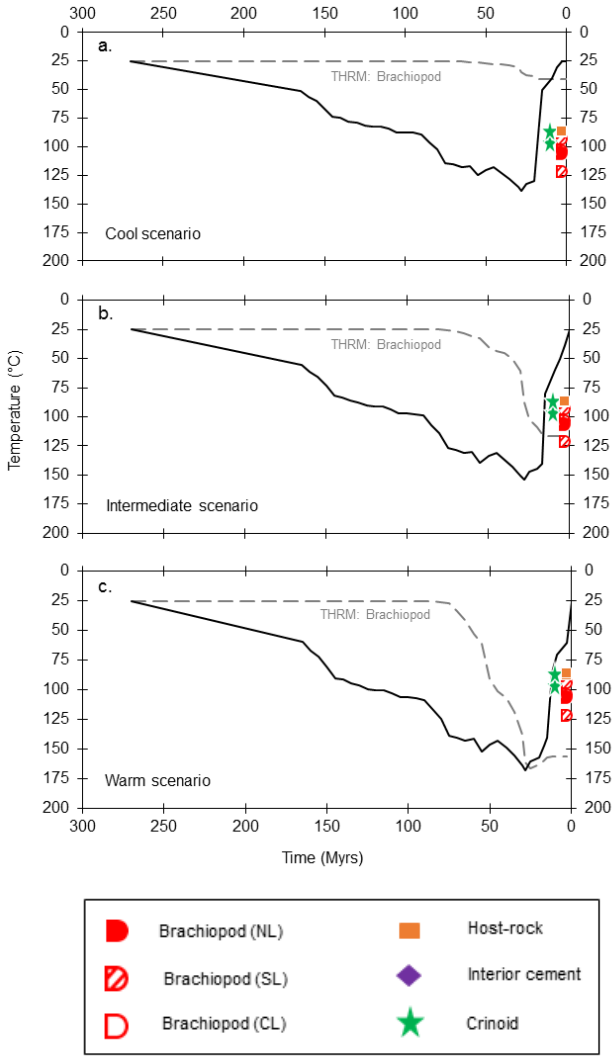

Fig. 6 Thermal history reordering models for the Quebrada de Portachuelo site, Venezuela. (a) Cool, (b) intermediate, and (c) warm temperature-time (T-t) histories for the Palmarito Formation marked by solid black lines. Thermal history reordering model (THERM) predictions are also shown (grey dashed lines). THRMs are initiated at 25 °C and progressively modeled based on first-order kinetics and Arrhenius parameters of a Permian brachiopod (Passey and Henkes, 2012; Henkes et al., 2014). Measured T(Δ_{47})s of different carbonate components are plotted on the y-axis for direct comparison to model predictions. Note that THRM predictions for the intermediate T-t history generally correspond with measured T(Δ_{47})s, but predictions for the cool and warm scenarios vary significantly.

assumption may be valid for well-preserved brachiopods, but metastable crinoids and host rock likely experienced open-system alteration. Hence, a different model simulation may be more appropriate to assess the extent of bond reordering in crinoids and host rock (see 'Comparing Carbonate Components' section).

6.2.2 Bird Spring Formation, Nevada

Henkes et al. (2014) previously reported T(Δ_{47})s of brachiopods and host rock with an associated THRM for the Bird Spring Formation at Arrow Canyon, Nevada. That work included low (~100 °C), intermediate (135 C°) and high (170 °C) peak temperature estimates, which were in part based on published CAI values. The THRM predictions for those 1D thermal histories varied from no bond reordering in the lowest temperature scenario to complete reordering and equilibration of clumped isotopes in the highest temperature scenario. Thus, it is necessary to revisit the model predictions as I present a new higher-resolution thermal history with peak temperature estimates of at least 170 °C, constrained by fluid inclusion measurements.

A THRM was generated for an intermediate and warm T-t scenario for the Bird Spring Formation at Arrow Canyon, Nevada (Fig. 7; termed THRM-Bird Spring in Table 2). The intermediate scenario serves as a minimum estimate of burial temperature because it achieves minimum peak temperature estimates based on fluid inclusion microthermometry data of 170 °C. In both the intermediate and warm T-t scenarios, THRMs predict that T(Δ_{47}) reached equilibrium with ambient burial temperature prior to

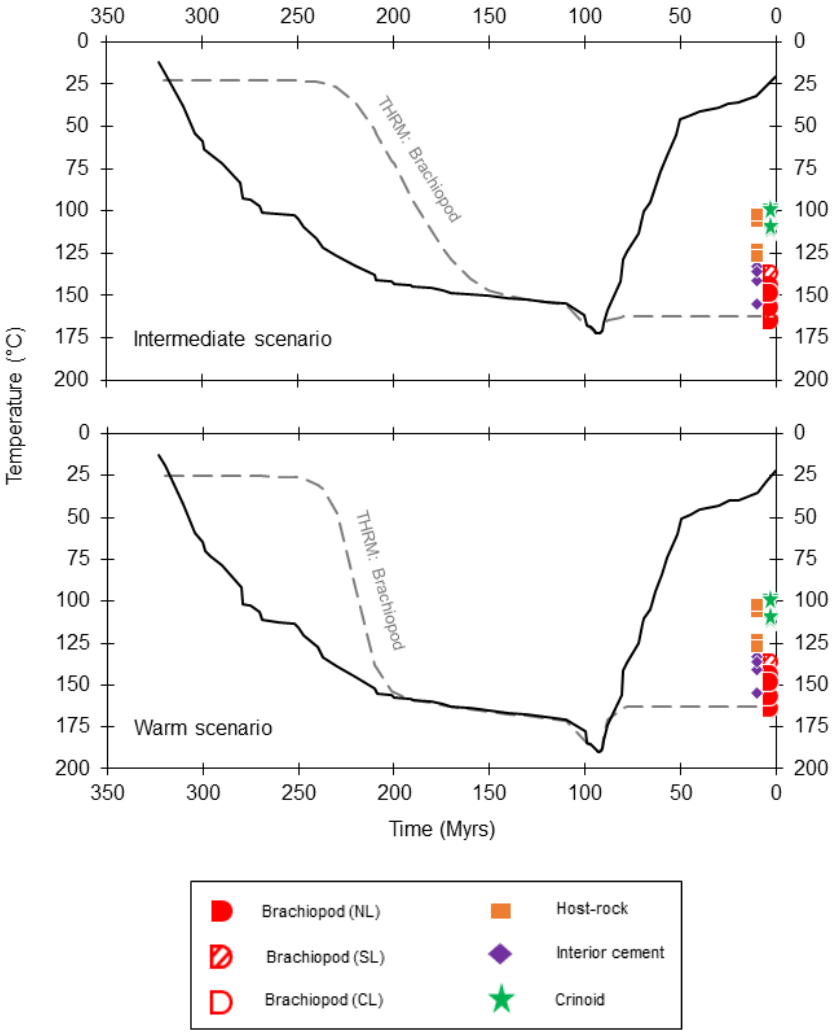

Fig. 7 Thermal history reordering models for Arrow Canyon, Nevada, USA. (a) Intermediate and (b) warm temperature-time (T-t) histories (solid black lines) for the Bird Spring Formation at Arrow Canyon, Nevada. Thermal history reordering model (THRM) predictions are also shown (grey dashed lines). THRMs are initiated at 25 °C and utilize first-order kinetics and previously determined Arrhenius parameters of a Permian brachiopod (Passey and Henkes, 2012; Henkes et al., 2014). Measured T(Δ_{47})s of different carbonate components are plotted on the y-axis for direct comparison with model predictions. Note that in both scenarios brachiopod T(Δ_{47})s are predicted to completely equilibrate with ambient burial temperature prior to recording cooling-rate-dependent blocking temperatures of ~160 °C, which are in general agreement with measured brachiopod T(Δ_{47})s. In contrast, THRM predictions based are 40-60 °C higher than average crinoid and host-rock T(Δ_{47})s.

recording a cooling-rate-dependent blocking temperature of 160 °C during exhumation. Both scenarios predict similar apparent T(Δ_{47})s because they both reach sufficiently-high burial temperatures (and dwelling times at those temperatures) to allow attainment of clumped isotope equilibration, and both scenarios have the same cooling rate. The predicted T(Δ_{47}) is also in agreement, within error, of measured T(Δ_{47})s of brachiopods. However, the measured clumped isotope temperatures of crinoids and host-rock are ~40-60 °C cooler than predicted T(Δ_{47})s based on THRMs using brachiopod reordering kinetics (Fig. 7). Thus, it is important to consider other possible scenarios that would result in these calcite components having final T(Δ_{47})s of ~100 °C.

6.3 Comparing Carbonate Components

6.3.1 General Constraints

As previously discussed, THRMs assume that samples are not recrystallized, and require an estimate of initial T(Δ_{47}). To better inform estimates of the latter value for crinoids, clumped isotope compositions of four Carboniferous crinoids were examined from the Eastern Shelf of the Midland Basin (Fig. A-4), which are expected to record stabilization temperatures (i.e., reflecting only HMC–dLMC transition, porosity-fill or other open-system alteration) because they were not deeply buried due to their position near the basin margin (Brown et al., 1973; Erxleben, 1974). T(Δ_{47})s of the four crinoids range from 16 to 86 °C (Table 3), confirming the complexity of open-system alteration of crinoids (e.g. Dickson, 2001), and suggesting that they can be altered soon after deposition in conditions similar to their mineralization temperature, or remain open to stabilization during shallow burial. The higher temperature samples are consistent

Sample ID	Formation	$\delta^{13}C_{calcite}$ (‰, VPDB)	$\delta^{18}O_{calcite}$ (‰, VPDB)	Δ_{47} (‰, CDES)*	Temp (°C)†	$\delta^{18}O_{water}$ (‰, VSMOW)§
CC-Cr1	Colony Creek Shale	-0.54	-8.39	0.714	16	-9
CC-Cr2	Colony Creek Shale	-1.18	-6.85	0.578	65	2
Js-Cr	Finis Shale	2.95	-7.42	0.536	86	4
PP-Cr	Palo Pinto Formation	-3.43	-6.40	0.674	28	-4

Note: There are currently no error estimations as n=1 for all samples.
*Presented in the carbon dioxide equilibrium scale (CDES; Dennis et al., 2011). All values have been adjusted + 0.092 to correct for fractionation during acid digestion.
†Temperatures are calculated using theoretical predictions of Schauble et al. (2006) corrected for an acid digestion temperature of 25 °C (Guo et al., 2009).
§Isotopic compositions of fluids are calculated using Friedman and O'Neil (1977).

Table 3 Isotopic compositions of Carboniferous crinoids from the Midland Basin, North-Central Texas

with stabilization or cementation as deep as ~2 km (assuming 25 °C surface temperature and ~25 °C/km geothermal gradient). Similarly, limestone matrix or host rock is subject to open-system alteration during shallow burial due to cementation, compaction, and induration and commonly yields T(Δ_{47})s ranging from 50-80 °C (e.g., Eiler, 2011). Thus, due to open-system alteration during early burial, THRMs for crinoids and host rock may more appropriately be constructed using clumped isotope temperatures reflecting this early stabilization phase, with higher initial temperatures than brachiopods.

6.3.2 Palmarito Formation, Venezuela

To account for open-system stabilization of crinoids and host-rock during early burial in the Palmarito Formation, Venezuela, a THRM with stabilization temperatures at model T-t steps nearest 50 and 75 °C (within 5 °C in all cases; THRM-Combination in Table 2) was generated. In these scenarios, predictions based on brachiopod reordering kinetics are complemented by simulations based on kinetics of an optical calcite and vein-filling spar (Passey and Henkes 2012). Due to chemical and optical heterogeneity,

reordering kinetics of the spar may reflect a combination of two end-member components, termed 'labile' and 'refractory' (Passey and Henkes, 2012) which are used here to explore the influence on THRM predictions of the range of observed kinetics from laboratory experiments.

In the thermal history reordering model it is obvious that different Arrhenius parameters result in substantially different predictions for the same T-t history (Fig. 8a-b). For example, in the Palmarito Formation thermal history, the predicted final $T(\Delta_{47})$ based on kinetics of the refractory and labile components of spar are unchanged or only subtly altered (i.e., from an initial temperature of 55 °C to a final temperature of 56 °C, and from 55 to 63 °C, for the refractory and labile kinetics, respectively). However, the predicted $T(\Delta_{47})$s based on kinetics for the optical calcite and brachiopod calcite are measurably changed from initial values (from 55 to 95 °C for the optical calcite kinetics, and from 55 to 145 °C for the brachiopod calcite kinetics). Note also that higher stabilization temperatures yield higher predicted $T(\Delta_{47})$s after burial and exhumation (Fig. 8). Thus, $T(\Delta_{47})$s of crinoids and host rock in the Palmarito Formation can be explained by higher initial $T(\Delta_{47})$s reflecting chemical stabilization and porosity-fill during early burial, for example at 50 or 75 °C, and greater resistance to C-O bond reordering during subsequent heating than brachiopods.

6.3.3 Bird Spring Formation, Nevada

A THRM was generated for the Bird Spring Formation, Nevada using the same stabilization temperatures (i.e., at model time steps nearest 50 and 75 °C) and laboratory-

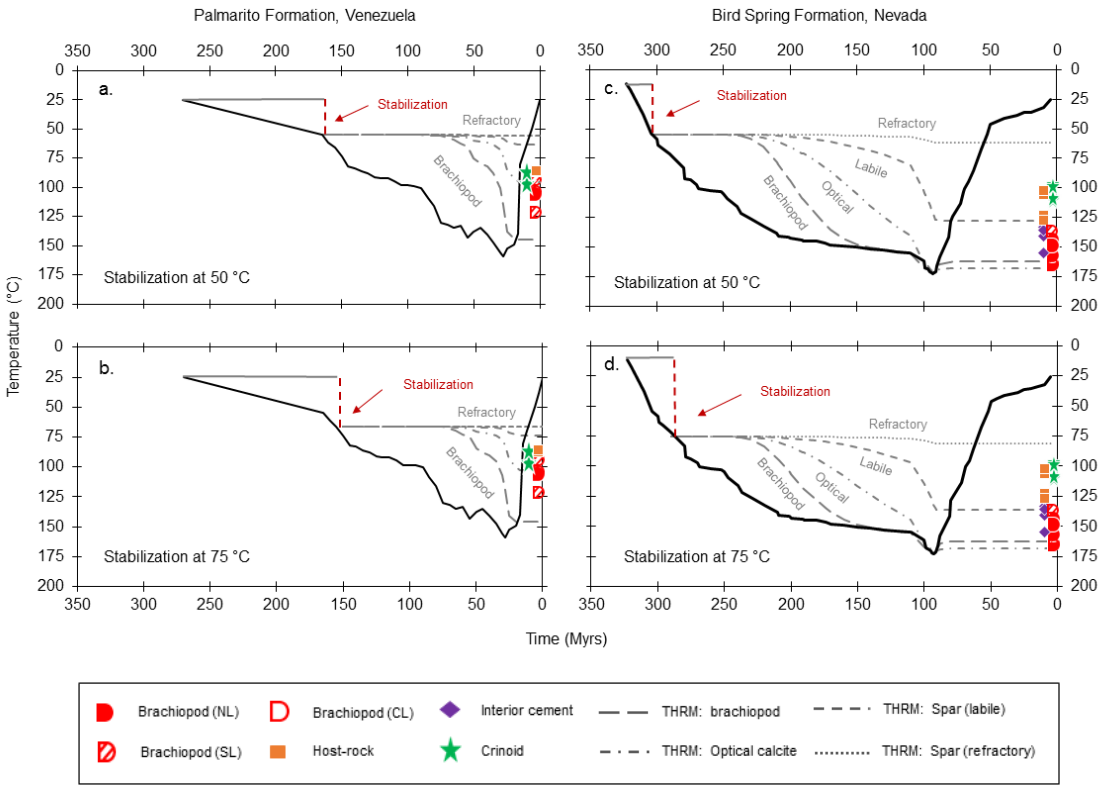

Fig. 8 Thermal history reordering models from stabilization temperatures. Temperature-time (T-t) plots for both the Palmarito (a,b) and Bird Spring (c,d) formations (solid black lines). Both localities also have thermal history reordering models (THRMs; grey dashed lines) based on first-order kinetics and previously determined Arrhenius parameters for a Permian brachiopod, optical calcite, and two components of a vein-filling spar (termed 'labile' and 'refractory'; Passey and Henkes 2012; Henkes et al., 2014). Measured T(Δ_{47})s of different carbonate components are plotted on the y-axis. To account for possible open-system inversion to low-Mg calcite and porosity-fill/cementation of crinoids and host rock, THRMs begin from higher initial temperatures of 50 and 75 °C. Note that in both localities crinoid and host rock T(Δ_{47})s can be achieved by having higher stabilization temperatures and an increased resistance to C-O bond reordering.

derived kinetics as for the Palmarito Formation. The THRM (THRM-Stabilization in Table 2) shows significant separation of $T(\Delta_{47})$-time paths for components with different bond reordering parameters (Fig. 8c-d). THRMs based on experimental brachiopod and optical calcite reordering kinetics predict that $T(\Delta_{47})$s equilibrated with ambient burial temperature during peak heating, and subsequently recorded a cooling-rate-dependent blocking temperature of ~160 °C. Thus, in each initial or stabilization temperature scenario (25, 50, or 75 °C), models based on brachiopod Arrhenius parameters predict the same blocking temperature. This is because the peak temperatures and dwelling times of the Bird Spring Formation T-t history are sufficiently high to allow $T(\Delta_{47})$s to reach equilibrium with ambient burial temperatures and subsequently record a $T(\Delta_{47})$ dependent on cooling rate. As a result, model simulations of brachiopod kinetic parameters for any prograde stabilization temperature (0-170 °C) predict the same ~160 °C blocking temperature, ~40-60 °C higher than measured crinoid and host-rock $T(\Delta_{47})$. In contrast, model predictions based on the more resistant labile and refractory components of the spar yield predicted $T(\Delta_{47})$s that are similar to or bracket the measured $T(\Delta_{47})$s of crinoids and host-rock (Figure 8c-d). Thus, assuming closed-system behavior during exhumation, the differences in component $T(\Delta_{47})$s can be explained by crinoids and host rock being more resistant to C-O bond reordering than brachiopods.

While the measured $T(\Delta_{47})$s and THRMs support the contention that host rock and crinoids are more resistant to C-O bond reordering than brachiopods, they do not totally rule out the possibility that crinoids and host rock recrystallized during retrograde

cooling (e.g., at ~100 °C). Such recrystallization is unlikely, however, given that the crinoids and host rock have varying minor and trace element chemistries (Table 1), reflecting stabilization / recrystallization under differing conditions as opposed to a single widespread event during exhumation. Also note that sampled crinoids from Arrow Canyon span a range of textural preservation states from highly micro-fractured (e.g., AR8 and AR12) to structurally well-preserved (e.g., AR 16), yet they yield effectively identical T(Δ_{47})s. A lack of resetting during exhumation also is suggested by clumped isotope measurements of host rock from cores at depth and equivalent exhumed outcrop samples from Oman, which yield the same T(Δ_{47}), suggesting that host rock did not reset during exhumation (Eiler, 2011). Thus, I suggest that crinoids and host-rock at Arrow Canyon did not recrystallize at ~100 °C during exhumation, but rather that their unique T(Δ_{47})s reflect a different susceptibility to C-O bond reordering. Ultimately, laboratory investigations of Arrhenius parameters of crinoids and other carbonate components will be required to test this hypothesis.

6.4 Bird Spring Formation Cements

6.4.1 Pore-filling Cements

Cements within articulate brachiopod shells occur in laterally-extensive horizons and are depleted in $\delta^{18}O_{calcite}$ and Sr (Table 1), indicating that they precipitated from meteoric fluids. Under cathodoluminescence microscopy, some cements show complex zonation (e.g., AC1 and AR13; Fig. A-5), indicating that they precipitated in varying redox conditions (e.g., Barnaby and Rimstidt, 1989) and perhaps over a range of shallow burial temperatures. Since powders for clumped isotope analyses were milled from the

central portion of the cements, they likely represent later and warmer stages of precipitation (i.e., such a pattern of increasing temperature of early cements towards the center of pores was observed by Huntington et al., 2011). Thus, because cements have higher formation temperatures than brachiopods but yield similar apparent $T(\Delta_{47})$s, they likely are more resistant to bond reordering than brachiopods. This argument assumes no open-system alteration during burial, which is supported by the fact that, except for sample AR3, meteoric pore-filling cements preserve fringing cements and zonations indicating preservation of primary textures.

6.4.2 Void-fill

$T(\Delta_{47})$s of macro-scale void-filling calcite (Fig. A-6) at Arrow Canyon (21 °C) indicate that dissolution voids occurred relatively recently at near Earth-surface temperatures. In addition, calculated $\delta^{18}O_{water}$ values are low (-13.1‰), consistent with precipitation from meteoric water recharged at high elevation. These results highlight the application of clumped isotope thermometry towards deciphering diagenetic histories of components which form during or after cooling. Primary or secondary calcite precipitated during cooling below blocking temperatures will preserve primary $T(\Delta_{47})$ (with respect to solid-state reordering) that can be used to infer the conditions of formation and isotopic composition of the parent fluid.

7. CONCLUSIONS

Apparent clumped isotope temperatures of carbonate components in the Palmarito Formation, Venezuela and the Bird Spring Formation, Nevada, USA are the result of 1) initial precipitation temperature and age, 2) timing, temperature, and extent of open-system alteration, and 3) solid-state reordering during burial, which depends on the T-t history and the degree of susceptibility to closed-system bond reordering of different calcite phases. Measured clumped isotope temperatures of texturally well-preserved brachiopods in the Palmarito and Bird Spring formations generally correspond to thermal history reordering model predictions based on laboratory-derived kinetics and independently compiled T-t histories. Model predictions suggest that Palmarito Formation brachiopods experienced partial reordering of clumped isotope temperatures that did not equilibrate at maximum burial temperature. In contrast, Bird Spring Formation brachiopods are predicted to have equilibrated at maximum burial temperatures and now reflect cooling rate dependent blocking temperatures.

A key finding in this study is that Bird Spring Formation crinoids and host rock, which experienced the same thermal history as brachiopods, yield 40-50 °C cooler clumped isotope temperatures. However, the differences in crinoids and host rock clumped isotope temperatures and brachiopod T(Δ_{47})s can be explained by stabilization of metastable HMC or aragonite and secondary pore-fill during early burial (e.g., at 50 or 75 °C) followed by a greater inherent resistance to C-O bond reordering during subsequent heating. Consistent with this hypothesis, the bond reordering kinetics

required for crinoids and host rock matrix to achieve their observed clumped isotope temperatures in the Bird Spring Formation are within the range of previously determined kinetic parameters. Similarly, bond reordering kinetics also can explain crinoid and host rock T(Δ_{47})s in the Palmarito Formation, Venezuela, assuming stabilization and cementation during early burial. A less likely, but alternative explanation for the differences in T(Δ_{47})s in the Bird Spring Formation is that crinoids and host rock experienced recrystallization during exhumation at ~100 °C. The observation of different temperatures in different components that experienced the same thermal history suggests that different carbonate components can act as independent geothermometers from the same rock. The primary limitation for applying THRMs in multiple carbonate components is independently constraining their stabilization temperatures and screening for subsequent recrystallization. Thus, future studies should emphasize materials that have constraints on these conditions.

REFERENCES

Barnaby, R.J., Rimstidt, J.D., Redox conditions of calcite cementation interpreted from Mn and Fe contents of authigenic calcites, 1989: Geological Society of America Bulletin, v. 101, p. 795-804.

Bergman, S.C., Huntington, K.W., Crider, J.G., 2013, Tracing paleofluid sources using clumped isotope thermometry of diagenetic cements along the Moab Fault, Utah: American Journal of Science, v. 313, p. 490-515.

Bermudez, M.A., Kohn, B.P., Van der Beek, P.A., Bernet, M., O'Sullivan, P.B., Shagam, R., 2010, Spatial and temporal patterns of exhumation across the Venezuelan Andes: Implications for Cenozoic Caribbean geodynamics: Tectonics, v. 29, TC5009, doi: 10.1029/2009TC002635.

Bischoff, W.D., Bertram, M.A., Mackenzie, F.T., Bishop F.C., 1993, Diagenetic stabilization pathways of magnesian calcites: Carbonates and Evaporites, v. 8, p. 82-89.

Bishop, J.W., Montañez, I.P., Gulbranson, E.L., Brenckle, P.L., 2009. The onset of mid-Carboniferous glacio-eustasy: Sedimentologic and diagenetic constraints, Arrow Canyon, NV: Palaeogeography, Palaeoclimatology, Palaeoecology, v. 276, p. 217-243.

Bishop, J.W., Montañez, I.P., Osleger, D.A., 2010, Dynamic Carboniferous climate change, Arrow Canyon, Nevada: Geosphere, v. 6, p. 1-34.

Brand, U., Posenato, R., Came, R., Affek, H., Angiolini, L., Azmy, K., Farabegoli, W., 2012, The end Permian mass extinction: a rapid volcanic CO_2 and CH_4-climatic catastrophe: Chemical Geology, v. 322, p. 121-144.

Brand, U., Veizer, J., 1986, Chemical diagenesis of a multicomponent system-1: Trace elements: Journal of Sedimentary Petrology, v. 50, p. 1219-1236.

Brenckle, P.L., Baesemann, J.F., Lane, H.R., West, R.R., Webster, G.D., Langenheim, R.L., Brand, U., Richards, B.C., 1997, Arrow Canyon, the Mid-Carboniferous boundary stratotype, Cushman Foundation Foraminiferal Research Supplement to Special Publications, v. 36, p 45-53.

Brown, L.F., Cleaves, A.W. II, Erxleben, A.W., 1973, Pennsylvanian depositional systems in north-central Texas: A guide for interpreting terrigenous clastic facies in a cratonic basin: Texas Bureau of Economic Geology Guidebook, v. 14, p. 4-6.

Budd, D.A., Frost, E.L., Huntington, K.W., Allwardt, P.F., 2013, Syndepositional deformation features in high-relief carbonate platforms: long-lived conduits for diagenetic fluids: Journal of Sedimentary Research, v. 82, p. 12-36.

Came, R.E., Eiler, J.M., Veizer, J., Azmy, K., Brand, U., Weidman, C.R., 2007, Coupling of surface temperatures and atmospheric CO_2 concentrations during the Palaeozoic era: Nature, v. 449, p. 198-202.

Cashman, P.H., Trexler, J.H., Jr., Davydov, V.I., Snyder, W.S., 2011a, Tectonostratigraphy of the Great Basin from the Antler orogeny through Pennsylvanian time, *in* Steininger, R., and Pennel, B., eds., Great Basin Evolution and Metallogeny: Reno, Geological Society of Nevada 2010 Symposium, p. 299-311.

Cashman, P.H., Villa, D.E., Taylor, W.J., Davidov, V.I., Trexler, J.H., Jr., 2011b, Late Paleozoic contractional and extensional deformation at Edna Mountain, Nevada: Geological Society of American Bulletin, v. 123, p. 651-668

Cassity, P.E., Langenheim, R.L., Jr, 1966, Pennsylvanian and Permian fusulinids of the Bird Spring Group from Arrow Canyon, Clark County, Nevada: Journal of Paleontology, v. 40, p. 931-968.

Colletta, B., Roure, F., De Toni, B., Loureiro, D., Passalacqua, H., Gou, Y., 1997, Tectonic inheritance, crustal architecture, and contrast in structural styles in the Venezuelan Andes: Tectonics, v. 16, p. 777-794.

Dale, A., John, C.M., Mozley, P.S., Smalley, P.C., Muggeridge, A.H., 2014, Time-capsule concretions: Unlocking burial diagenetic processes in the Mancos Shale using carbonate clumped isotopes: Earth and Planetary Science Letters, v. 394, p. 30-37.

Dennis, K.J., Affek, H.P., Passey, B.H., Schrag, D.P., Eiler, J.M., 2011, Defining an absolute reference frame for 'clumped' isotope studies of CO2: Geochimica et Cosmochimica Acta, v. 75, p. 7117-7131.

Dennis, K.J., Schrag, D.P., 2010, Clumped isotope thermometry of carbonatites as an indicator of diagenetic alteration: Geochimica et Cosmochimica Acta, v. 74, p. 4110-4122.

Dickinson, W.R., 2006, Geotectonic evolution of the Great Basin: Geosphere v. 2, p. 353-368.

Dickinson, W.R., and Lawton, T.F., 2003, Sequential intercontinental suturing as the ultimate control for Pennsylvanian Ancestral Rocky Mountains deformation: Geology, v. 31, p. 609-612.

Dickson, J.A.D., 2001, Diagenesis and crystal caskets: echinoderm Mg calcite transformation, Dry Canyon, New Mexico, U.S.A.: Journal of Sedimentary Research, v. 71, p. 764-777.

Dunham, R.J., 1962, Classification of carbonate rocks according to depositional texture, *in* Ham, W.E. eds., Classification of carbonate rocks-a symposium: American Association of Petroleum Geologists Memoir v. 1, p. 108-121.

Eiler, J.M., 2007, "Clumped-isotope" geochemistry-the study of naturally-occurring, multiply-substitute isotopologues: Earth and Planetary Science Letters, v. 262, p. 309-327.

Eiler, J.M., 2011, Paleoclimate reconstruction using carbonate clumped isotope thermometry: Quaternary Science Reviews, v. 30, p. 3675-3588.

Epstein, A.G., Epstein, J.B., Harris, L.D., 1977, Conodont color alteration-an index to organic metamorphism: U.S. Geological Survey Professional Paper v. 995, p. 27.

Erxleben, A.W., 1974, Depositional systems in the Pennsylvanian Canyon Group, north-central Texas, [Ph.D dissertation], The University of Texas at Austin, p. 11

Farley, K.A., 2002, (U-Th)/He dating: Techniques, calibrations, and applications: Reviews in Mineralogy and Geochemistry, v. 48, p. 559-577.

Finnegan, S., Bergmann, K., Eiler, J.M., Jones, D.S., Fike, A., Eisenman, I, Hughes, C., Tripati, A.K., Fischer, W.W., 2011, The magnitude and duration of the late Ordovician-early Silurian glaciation: Science, v. 331, p. 903-906.

Fleck, R.J., Carr, M.D., 1990, The age of the Keystone Thrust: Laser-fusion $^{40}Ar/^{39}Ar$ dating of Foreland Basin Deposits, southern Spring Mountains, Nevada: Tectonics, v. 9, p. 467-476.

Friedman, I., O'Neil, J.R., 1977, Data of Geochemistry, Sixth Edition, Chapter KK, Compilation of stable isotope fractionation factors of geochemical interest. U.S., Geological Survey Professional Paper 440-KK, U.S., Government Printing Office, Washington.

Ghosh, P., Adkins, J., Affek, H., Balta, B., Guo, W.F., Schauble, E.A., Schrag, D., Eiler, J.M., 2006, 13C-18O bonds in carbonate minerals: a new kind of paleothermometer: Geochimica et Cosmochimica Acta, v. 70, p. 1439-1456.

Gleadow, A.J.W., Duddy, I.R., Green, P.F., Lovering, J.F., 1986, Confined track lengths in apatite: a diagnostic tool for thermal history analysis: Contributions to Mineralogy and Petrology, v. 94, p. 405-415.

Goldstein, R.H., Reynolds, T.J., 1994, Systematics of fluid inclusions in diagenetic minerals: Society for Sedimentary Geology short course, v. 31, p. 199.

Grossman, E.L., 2012, Oxygen isotope stratigraphy, *in* Gradstein, F.M., Ogg, J.G., Smith, A., eds., A New Geologic Time Scale, Cambridge University Press.

Grossman, E.L., 1994, The carbon and oxygen isotope record during the evolution of Pangea: Carboniferous to Triassic, *in* Klein, G.D. eds., Pangea: Paleoclimate Tectonics, and Sedimentation During Accretion, Zenith, and Breakup of a Supercontinent: Geological Society of America Special Paper, v. 288, p. 207-228.

Guo, W., Mosenfelder, J.L., Goddard, W.A., Eiler, J.M., 2009, Isotopic fractionations associated with phosphoric acid digestion of carbonate minerals: Insights from first-principles theoretical modeling and clumped isotope measurements: Geochimica et Cosmochimica Acta, v. 73, p. 7203-7225.

Henkes, G.A., Passey, B.H., Wanamaker, A.D. Jr, Grossman, E.L., Ambros, W.G., Carroll, M.L., 2013, Carbonate clumped isotope compositions of modern marine mollusk and brachiopod shells: Geochimica et Cosmochimica Acta, v. 106, p. 307-325.

Henkes, G.A., Passey, B.H., Grossman, E.L., Shenton, B.J., Perez-Huerta, A., Yancey, T.E., 2014, Temperature time limits for preservation of primary calcite clumped isotope paleotemperatures, Geochimica et Coscmochimica Acta., doi: 10.1016/j.gca.2014.04.040

Huntington, K.W., Budd, D.A., Wernicke, B.P., Eiler, J.M., 2011, Use of clumped-isotope thermometry to constrain the crystallization temperature of diagenetic calcite: Journal of Sedimentary Research, v. 81, p. 656-669.

Kluth, C.F., 1986, Plate tectonics of the Ancestral Rocky Mountains, in Peterson, J,A., ed., Paleotectonics and sedimentation in the Rocky Mountain region, United States: American Association of Petroleum Geologists Memoir, v. 41, p. 353-369.

Kluth, C.F., and Coney, P.J., 1981, Plate tectonics of the Ancestral Rocky Mountains: Geology, v. 9, p. 10-15.

Kronenberg, A.K., Yund, R.A., Giletti, B.J., 1984, Carbon and oxygen diffusion in calcite: Effects of Mn content and pH_20: Physics and Chemistry of Minerals, v. 11, p. 101-112.

Lane, H.R., Brenckle, P.L., Baesemann, J.F., Richards, B., 1999, The IUGS boundary in the middle of the Carboniferous: Arrow Canyon, Nevada, USA: Episodes, v. 22, p. 76-105.

Langenheim, R.L. Jr, Carss, B.W., Kennerly, J.B., McCutcheon, V.A., Waines, R.H., 1962, Paleozoic section in Arrow Canyon Range, Clark County, Nevada: American Association of Petroleum Geologists Bulletin, v. 46, p. 592-609.

Laya, J.C., Tucker, M.E., 2012, Facies analysis and depositional environment of Permian carbonates in the Venezuelan Andes: Palaeogeographic implications to Northern Gondwana: Palaeogeography, Palaeoclimatology, Palaeoecology, v. 332, p. 1-26.

Laya, J.C, Tucker, M.E., Grocke, D.R., Perez-Huerta, A., 2013a, Carbon, oxygen and strontium isotopic composition of low-latitude Permian carbonates: Climate proxies of tropical Pangea, *in* A. Gasiewicz, M. Slowakiewicz eds., Late Palaeozoic Climate cycles: Their evolutionary, sedimentological and economic impact, Geological Society of London Special Publication, v. 376, p. 1-19.

Laya, J.C., Tucker, M.E., Perez-Huerta, A., 2013b, Metre-scale cyclicity in Permian ramp carbonates of equatorial Pangea (Venezuelan Andes): Implications for sedimentation under tropical Pangea conditions: Sedimentary Geology, v. 292, p. 15-35.

Loyd, S.J., Corsetti, F.A., Eiler, J.M., Tripati, A.K., 2012, Determining the diagenetic conditions of concretion formation: Assessing temperatures and pore water using clumped isotopes: Journal of Sedimentary Research, v. 82, p. 1006-1016.

Loyd, S.J., Dickson, J.A.D., Scholle, P.A., Tripati, A.K., 2013, Extensive, uplift-related and non-fault-controlled spar precipitation in the Permian Capitan Formation: Sedimentary Geology, v. 298, p. 17-27.

Machel, H.G., 1983, Cathodoluminescence in calcite and dolomite and its chemical interpretation: Geoscience Canada, v. 12, p. 139-147

Mann, P., Escalona, A., Castillo, M.V., 2006, Regional geologic and tectonic setting of the Maracaibo supergiant basin, western Venezuela: The American Association of Petroleum Geologists Bulletin, v. 90, p. 445-477.

Martin, L.G., Montañez, I.P., Bishop, J.W., 2012, A paleotropical carbonate-dominated archive of Carboniferous icehouse dynamics, Bird Spring Fm., southern Great Basin, USA, Palaeogeography, Palaeoclimatology, Palaeoecology, v 329-330, p. 64-82.

Mii, H.S., Grossman, E.L., Yancey, T.E., 1999, Carboniferous isotope stratigraphies of North America: implications for Carboniferous paleooceanography and Mississippian glaciation: Geological Society of America Bulletin, v. 111, p. 960-973.

Page, W.R., and Dixon, G.L., 1997, Geologic framework of the Arrow Canyon area, Clark County, Nevada: Cushman Foundation Foraminiferal Research Supplement to Special Publication, v. 36, p. 5-12.

Page, W.R., Lundstrom, S.C., Harris, A.G., Langenheim, V.E., Workman, J.B., Mahan, S.A., Paces, J.B., Dixon, G.L., Rowley, P.D., Burchfiel, B.C., Bell, J.W., Smith, E.I., 2005, Geologic and geophysical maps of the Las Vegas 30' x 60' quadrangle, Clark and Nye Counties, Nevada, and Inyo County, California: U.S. Geological Survey Scientific Investigations Map 2814.

Passey, B.H., Henkes, G.A., 2012, Carbonate clumped isotope bond reordering and geospeedometry: Earth and Planetary Science Letters, v. 352, p. 223-236.

Passey, B.H., Levin, N.E., Cerling, T.E., Brown, F.H., Eiler, J.M., 2010, High-temperature environments of human evolution in East Africa based on bond ordering in paleosol carbonates: Proceedings of the National Academy of Sciences of the United States of America, v. 107, p. 11245-11249.

Peters, K.E., Walters, C.C., Moldowan, J.M., 2005, The biomarker guide, Cambridge University Press, Cambridge, UK.

Pierson, B.J., 1981, The control of cathodoluminescence in dolomite by iron and manganese: Sedimentology, v. 28, p, 601-610.

Popp, B.N., Anderson, T.F., Sandberg, P.A., 1986, Brachiopods as indicators of original isotopic compositions in some Paleozoic limestones: Geological Society of America Bulletin, v. 97, p. 1262-1269.

Richards, B.C., Lane, R.H., Brenckle, P.L., 2002, The IUGS Mid-Carboniferous boundary stratotype section and point at Arrow Canyon, Nevada, USA, *in* Hills, L.V., et al., eds., Carboniferous and Permian of the world: Canadian Society of Petroleum Geologists Memoir, v. 19, p. 802-831.

Savarese, M., Dodd, J.R., Lane, N.G., 1997, Taphonomic and sedimentologic implications of crinoid intraskeletal porosity: Lethaia, v. 29, p. 141-156.

Schauble, E.A., Ghosh, P., Eiler, J.M., 2006, Preferential formation of ^{13}C-^{18}O bonds in carbonate minerals, estimated using first-principles lattice dynamics: Geochimica et Cosmochimica Acta, v. 70, p. 2510-2529.

Schmoker, J.W., Halley, R.B., 1982, Carbonate porosity versus depth: a predictable relation for South Florida: American Association of Petroleum Geologists Bulletin, v. 66, p. 2561-2570.

Selley, R.C., 1998, Elements of petroleum geology, Academic Press, San Diego, Ca.

Smith, A.B., 1990, Biomineralization in echinoderms, *in* Carter, J.G., eds., Skeletal Biomineralization: Patterns, Processes and Evolutionary Trends, v. 1, p. 413-443.

Stevens, C.H. and Stone, P., 2007, The Pennsylvanian-Early Permian Bird Spring Carbonate Shelf, Southeastern California: Fusulinid Biostratigraphy, Paleogeographic Evolution, and Tectonic Implications: The Geological Society of America Special Paper, v. 429.

Sturmer, D.M., 2012, Stable carbon isotope chemostratigraphy and tectonic setting of the Pennsylvanian Ely-Bird Spring Basin, Nevada and Utah: interpreting three-dimensional basin evolution using multiple stratigraphic techniques [Ph.D dissertation]: Reno, University of Nevada, Reno, p. 378.

Swanson, E.M., Wernicke, B.P., Eiler, J.M., Losh, S., 2012, Temperatures and fluids on faults based on carbonate clumped-isotope thermometry: American Journal of Science, v. 312, p. 1-21.

Sweeney, J.J., Burnham, A.K., 1990, Evaluation of a simple model of vitrinite reflectance based on chemical kinetics: American Association of Petroleum Geologists Bulletin, v. 74, p. 1559-1570.

Thiagarajan, N.J., Adkins, J., Eiler, J.M., 2011, Carbonate clumped isotope thermometry of deep-sea corals and implications for vital effects: Geochimica et Cosmochimica Acta, v. 75, p. 4416-4425.

Trexler, J.H., Jr., Cashman, P.H., Snyder, W.S., and Davydov, V.I., 2004, Late Paleozoic tectonism in Nevada: Timing, kinematics, and tectonic significance: Geological Society of America Bulletin, v. 116, p. 525-538.

Veizer, J., Davin, A., Azmy, K., Bruckschen, P., Buhl, D., Bruhn, F., Carden, G.A.F., Diener, A., Ebneth, S., Godderis, Y., Jasper, T., Korte, C., Pawellek, F., Podlaha,

O.G., Straus, H., 1999, $^{87}Sr/^{86}Sr$, $\delta^{13}C$, and $\delta^{18}O$ evolution of Phanerozoic seawater: Chemical Geology, v. 161, p. 59-88.

APPENDIX A

Thermal History Workflows

Palmarito Formation, Venezuela

The 1D thermal history for the Palmarito Formation is modified from Callejon et al. (2003) to incorporate the additional burial depth of the Palmarito Formation. The additional thickness of the Palmarito Formation at the Quebrada de Portachuelo varies during compaction from 860.8 m (assuming initial 50 % carbonate porosity) to 468.7 m (present day thickness; Laya et al., 2013b) according to porosity versus depth observations of Schmoker and Halley (1982). Because Callejon et al. (2003) only reported burial depths, I also applied geothermal gradients to acquire a T-t history. For the intermediate T-t scenario, geothermal gradients during Jurassic rifting are 35 °C followed by 28 °C through present day. For the cool scenario the geothermal gradient during Jurassic rifting is 30 °C followed by a 25 °C gradient through present day. The warm scenario utilized a geothermal gradient of 40 °C during the Jurassic and 30 °C to present day.

The cooling history for the thermal model is drawn directly from apatite-fission track data from a sandstone in the La Quinta Formation (which directly overlies the Palmarito Formation; Bermudez et al. (2010). The intermediate scenario follows their 'most likely' exhumation path. The cool scenario draws from the most rapid exhumation path and the warm scenario is from the latest exhumation possible path (e.g., at higher temperatures for longer amount of time).

Bird Spring Formation, Nevada

The 1D basin model for the Mississippian-Pennsylvanian boundary at Arrow Canyon, Nevada was compiled by Tom Becker using ExxonMobil's proprietary Stellar^{TM} basin modeling software. The boundary conditions for creating the thermal histories include basal heat flow and surface temperature, which are dependent on latitude and elevation (relative to modern sea level). These boundary conditions are convolved with lithology dependent thermal conductivities and their characteristic radiogenic heat production. The prograde thermal history is constructed using thicknesses, lithologies, and ages of overlying stratigraphic formations, which were compiled from regional geologic maps of Page et al. (1992) and Page et al. (2005). The modeling software incorporates a lithology-dependent decompaction of formation thicknesses, providing a more accurate approximation of burial depth and porosity-dependent thermal conductivity through time. Basal heat flow parameters were selected at different times during the burial history based on the type of tectonic setting (i.e., Mississippian to early Cenozoic foreland basin of 55 mW/m^2, Neogene extension, 90 mW/m^2). After an initial simulation, basal heat flow parameters were subtly increased to 60 mW/m^2 during the foreland phase based on minimum peak temperature estimates provided by optical fluid inclusion data, indicating that the formation reached at least 170 °C during burial. The new peak temperature estimates from optical fluid inclusions are consistent with the upper limits of previously published conodont alteration index data (personal communication B. Wardlaw, 2013), and while the number of samples analyzed for inclusions is relatively small, it provides a significant improvement on

previous peak temperature estimates. Cooling history at Arrow Canyon is built on the observation that the youngest concordantly folded strata in the region are early-Late Cretaceous (Fleck and Carr, 1990), which implies timing of deformation. Apatite-fission track thermochronology is currently in progress to further refine the cooling history.

APPENDIX B

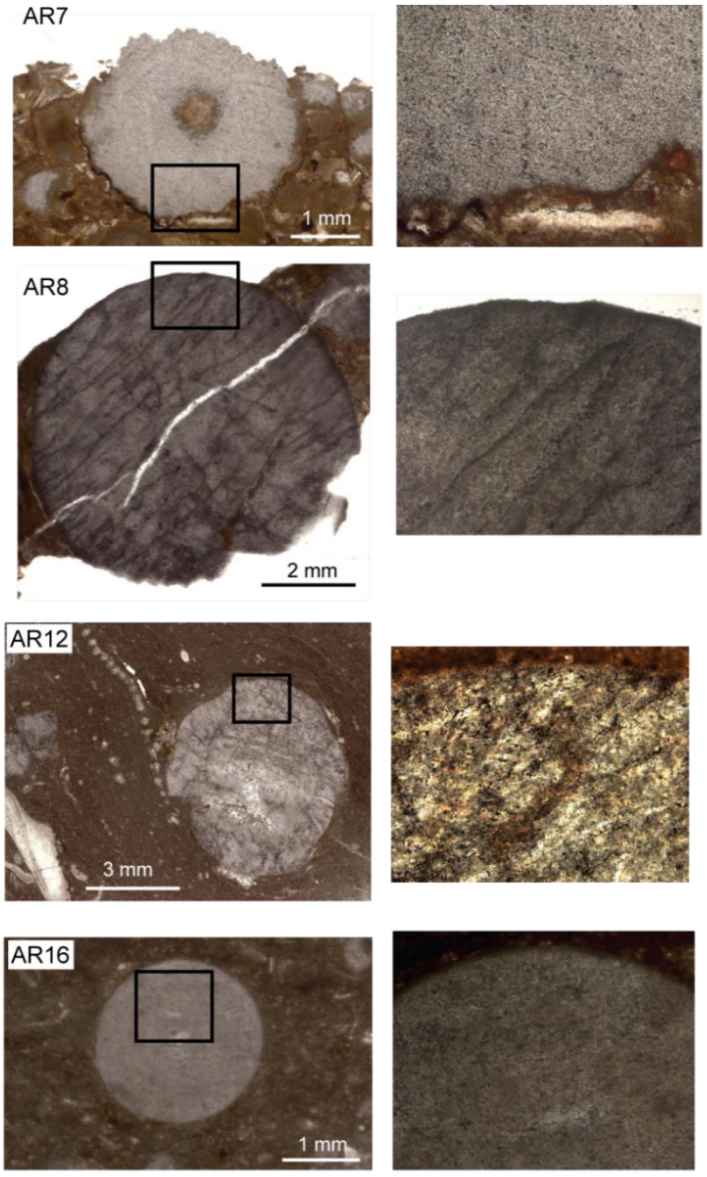

Fig. A-1. Thin section scans and associated plane light images of representative crinoids from the Bird Spring Formation, at Arrow Canyon, Nevada, USA. Isotopic and elemental analyses of samples AR7, AR8, and AR16 are from these and other adjacent crinoid ossicles. Plane light images have a scale of ~1.2 mm.

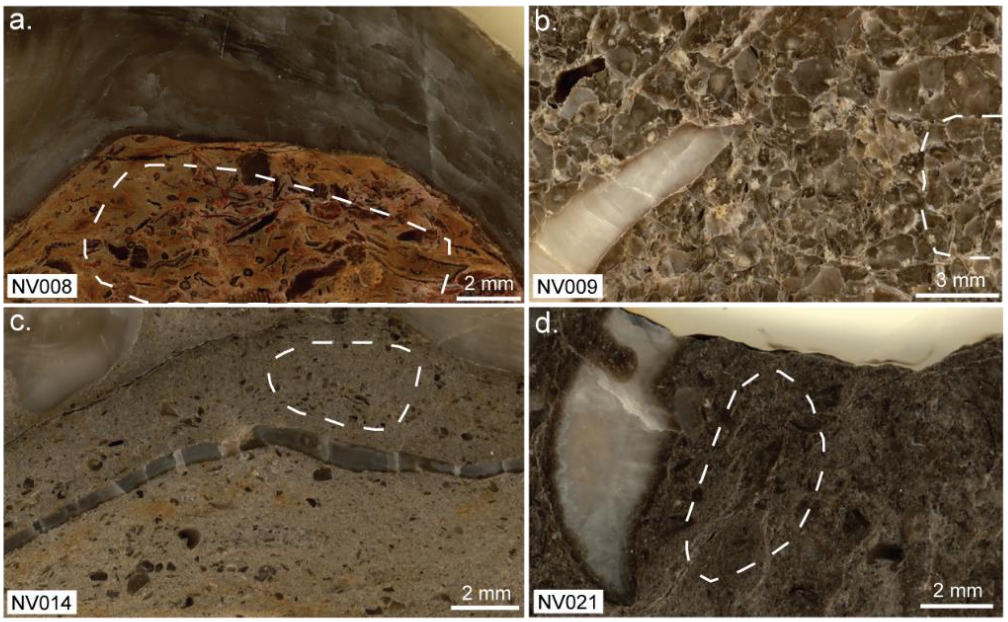

Fig. A-2**.** Thin section scans of samples NV008: a bioclastic wackestone (a), NV009: packestone (b), NV014: bioclastic wackestone (c), and NV021: bioclastic packestone (d) from the Bird Spring Formation at Arrow Canyon, NV. White dashed lines indicate areas that were micro-sampled for elemental and isotopic analysis to complement analyses of brachiopod shells. Samples are classified according to Dunham (1962).

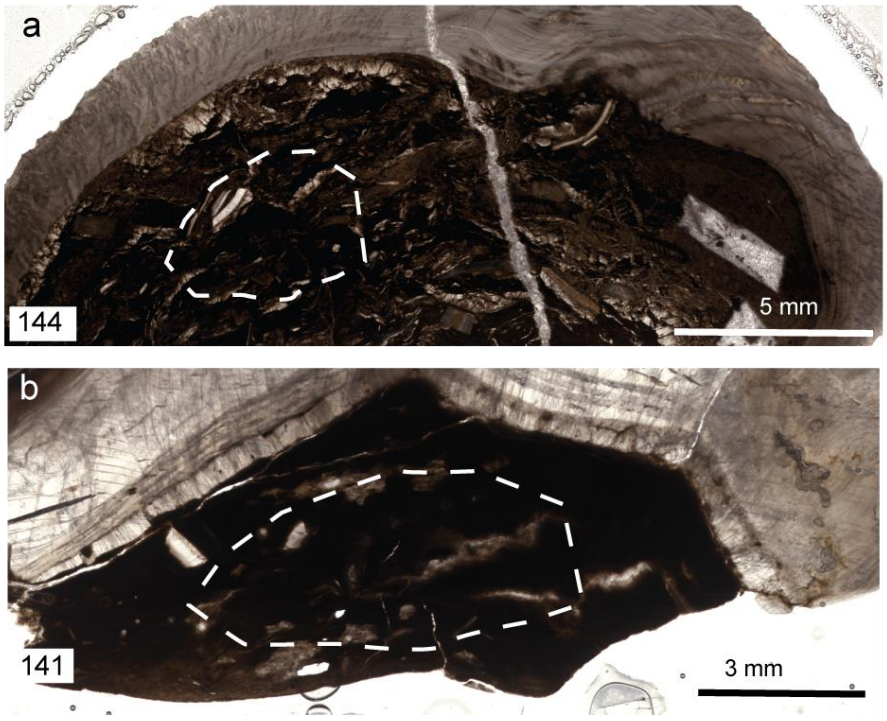

Fig. A-3. Photomicrographs of samples (a) 144 (wackestone) and (b) 141 (wackestone) from Quebrada de Portachuelo in the Palmarito Formation, Venezuela. White dashed lines indicate areas that were micro-sampled for elemental and isotopic analysis.

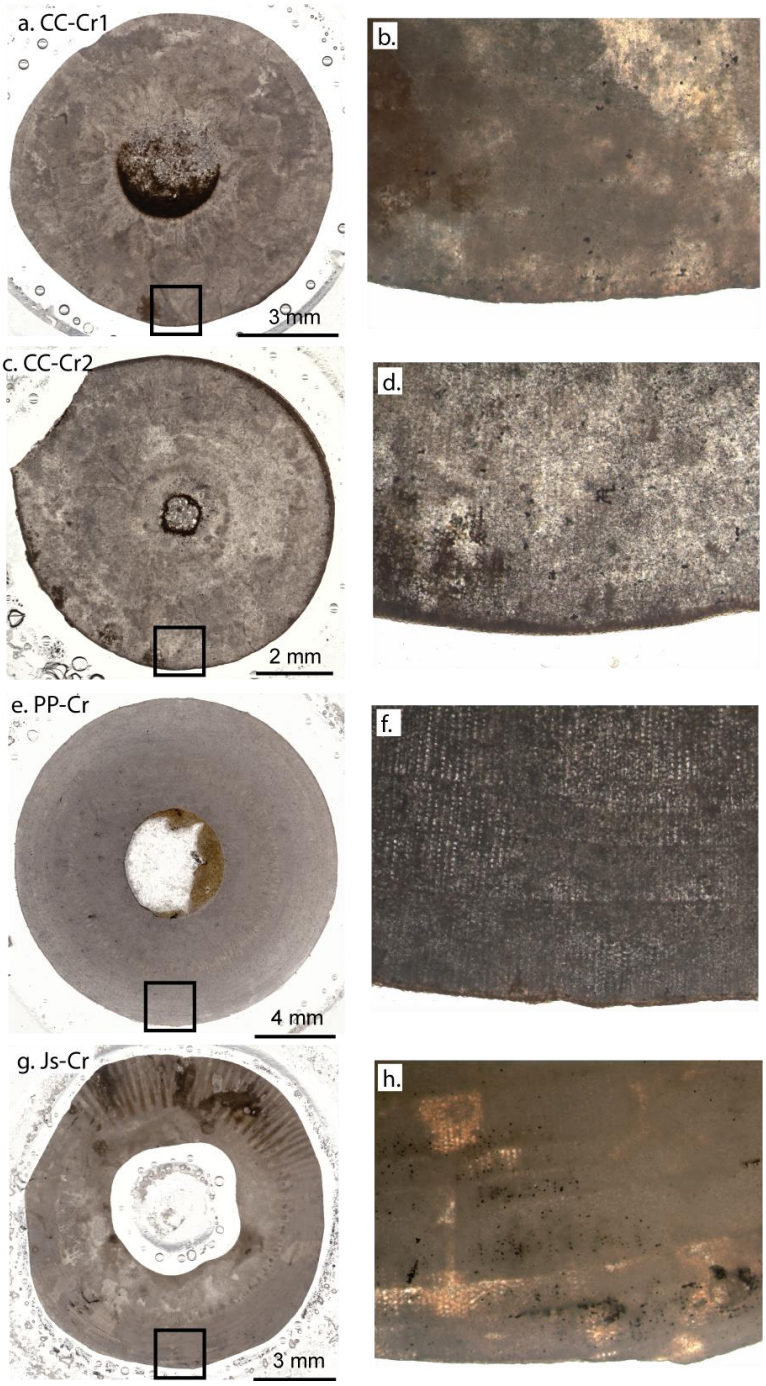

Fig. A-4. Thin section scans and associated plane light images of crinoids from the Eastern Shelf of the Midland Basin, Texas, USA. Scale for the plane light images is ~1.2 mm.

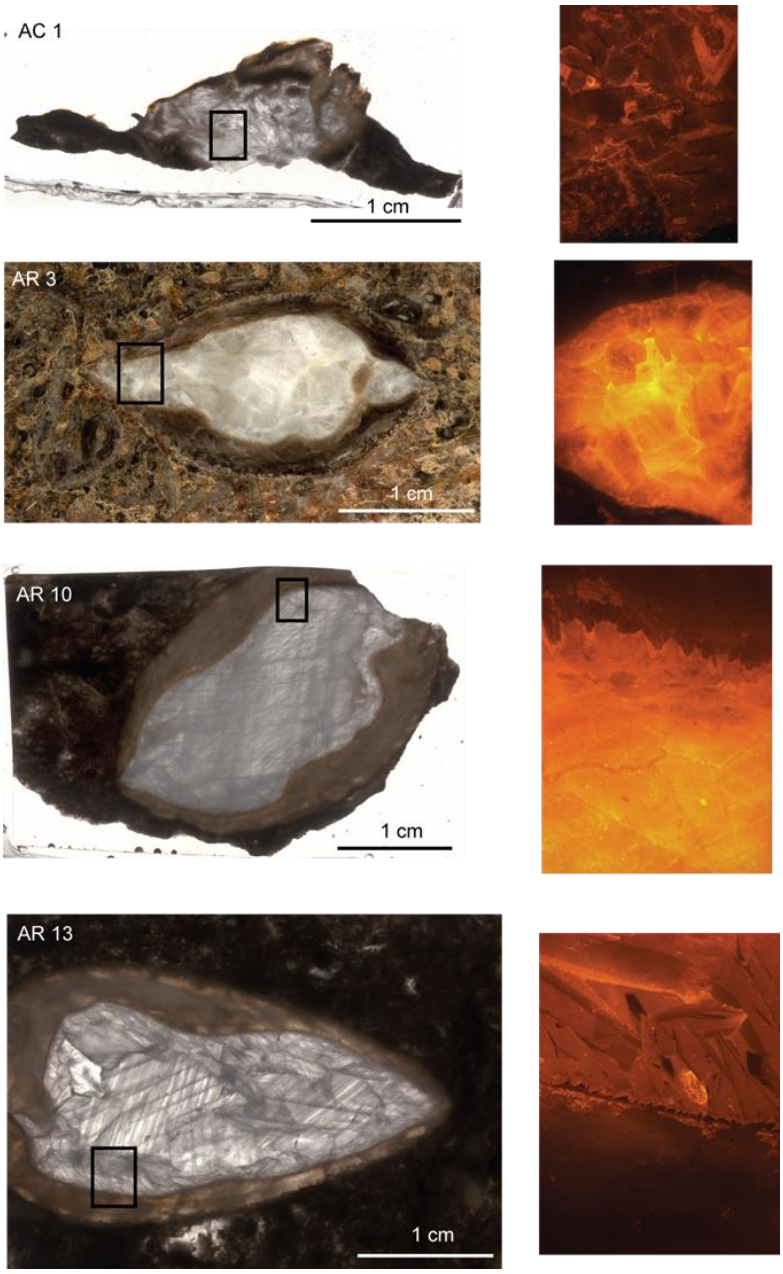

Fig. A-5. Thin section scans and cathodoluminescent images of pore-filling cements inside articulated brachiopod shells from the Bird Spring Formation at Arrow Canyon, Nevada, USA. Cathodoluminescence images have a scale of 2.2 mm.

Fig. A-6. Image of sample AR2 collected from modern dissolution veins that cross cut the Bird Spring Formation. Macro-calcite crystals formed in the vugs were collected and analyzed.